RESEARCH

Report No. UT-10.14

LABORATORY TESTING AND FINITE ELEMENT MODELING OF PRECAST BRIDGE DECK PANEL TRANSVERSE CONNECTIONS

Prepared For:

Utah Department of Transportation Research Division

Submitted By:

Utah State University
Department of Civil & Environmental Engineering

Authored By:

Scott Porter; J. Logan Julander
Marvin Halling; Paul Barr; Hugh Boyle

August 2010

UDOT
CONNECTING COMMUNITIES
Utah Department of Transportation-Research Division
4501 South 2700 West, Box 148410 - Salt Lake City, Utah 84114-8410

THIS PAGE INTENTIONALLY LEFT BLANK

1. Report No. UT-10.14	2. Government Access No.	3. Recipient's Catalog No.

4. Title and Subtitle	5. Report Date / 6. Performing Organization Code
Laboratory Testing and Finite Element Modeling of Precast Bridge Deck Panel Transverse Connections	5. Report Date August 6, 2010 6.Performing Organization Code
7. Author Scott Porter, J. Logan Julander, Marvin W. Halling, Paul Barr, Hugh Boyle	8.Performing Organization Report No.
9.Performing Organization Name and Address Utah State University Department of Civil & Environmental Engineering 4110 Old Main Hill Logan, UT 84322	10. Work Unit No. 11. Contract or Grant No.
12. Sponsoring Agency Name and Address Utah Department of Transportation 4501 South 2700 West Salt Lake City, Utah 84114-8410	13.Type of Report and Period Covered Final. 2008-2010 14.Sponsoring Agency Code

15. Supplementary Notes

Prepared in cooperation with the Utah Department of Transportation

16. Abstract

Precast bridge deck panels are increasingly used to reduce construction times and associated traffic delays as part of many DOT's push for accelerated bridge construction. They allow a bridge deck to be built or replaced in days instead of months. Despite the obvious benefits, the connections between panels have had a history of service failure problems.

To evaluate service and ultimate capacities of existing and proposed connections, full scale shear and flexural tests were performed at Utah State University on several types of precast bridge deck connections. These tests focused on the determination of ultimate and cracking strengths of five connections. These five connections were a welded connection anchored using nelson studs, a welded connection with embedded rebar used to anchor the plates, a conventionally post tensioned connection, and two variations of a newly proposed post tensioned curved bolt connection.

The welded rebar connection was shown to be significantly stronger than the welded stud connection. It failed at 2.7 times the moment failing the welded stud connection cracked at 2.1 times the load cracking the welded stud connection. The curved bolt connections were also shown to be a good alternative to conventional post tensioning. The longer connections had slightly higher flexural capacities than the post tensioned connections and cracked at 0.75 times the moment cracking the post tensioned specimens.

Finite element analysis models were used to verify the results. These models were made using Ansys. The finite element results closely matched the laboratory results.

17. Key Words	18.Disrtibution Statement	23. Registrant's Seal
Accelerated Bridge Construction, Precast Deck Panels, Transverse Connections, Post Tensioning, Curved Bolt, Welded Stud, Welded Rebar, Shear, Flexure	UDOT Research Division 4501 South 2700 West-box 148410 Salt Lake City, Utah 84114	

19. Security Classification	20. Security Classification	21. No. of Pages	22. Price
Unclassified	Unclassified	119	

THIS PAGE INTENTIONALLY LEFT BLANK

DISCLAIMER

"The authors alone are responsible for the preparation and accuracy of the information, data, analysis, discussions, recommendations, and conclusions presented herein. The contents do not necessarily reflect the views, opinions, endorsements, or policies of the Utah Department of Transportation of the US Department of Transportation. The Utah Department of Transportation makes no representation or warranty of any kind, and assumes no liability therefore."

THIS PAGE INTENTIONALLY LEFT BLANK

ACKNOWLEDGMENTS

The authors would like to acknowledge and thank UDOT and the Utah Transportation Center (UTC) for funding this research. We would particularly like to acknowledge Daniel Hsiao, Sr. Project Manager of UDOT's Research Division who managed this project from UDOT.

We would also like to thank Ken Jewkes and Wes Davidson for the use of their lab equipment and help with construction and testing. Their help in developing test setups and constructing panels was extremely valuable.

THIS PAGE INTENTIONALLY LEFT BLANK

TABLE OF CONTENTS

TABLE OF FIGURES

TABLE OF TABLES

THIS PAGE INTENTIONALLY LEFT BLANK

EXECUTIVE SUMMARY

Precast concrete bridge deck panels are being heavily used by UDOT in ABC (Accelerated Bridge Construction) projects. These panels allow bridge decks to be completed in days instead of months, significantly reducing construction times and associated traffic problems and bridge closures. Unfortunately, precast concrete bridge deck panels also have problems with cracking and other service issues – especially at connections between panels. These problems limit the life expectancy of ABC bridges.

To improve precast panels and determine optimal panel connections, this research project looked at female-to-female transverse (perpendicular to girders) connections between full-depth precast concrete bridge deck panels.

Several connection types were tested. They were UDOT's standard welded stud and post tensioned connections, a welded rebar connection similar to the welded stud connection, and two variations of a newly proposed curved bolt connection that provides post tensioning.

Connections were tested in shear, cyclic shear, and flexure in full scale tests. Ultimate failure loads were recorded along with cracking loads, the type of cracking, and deflections. These results were compared to finite element analysis models.

The welded rebar connection is a significant improvement over the welded stud connection. It did not fail in the connection in shear testing. In flexure, it held 2.7 times the ultimate capacity of the welded stud connection and 1.05 times the capacity of the post tensioned connection. This connection cracked in flexure at more than double the load required to crack the welded stud specimens and 0.88 times the load that cracked the post tensioned flexural specimens.

The post tensioned connection performed the best in shear of any connection tested and had essentially the same capacity in flexure as the welded rebar connection. It had the highest shear strength, 2.0 times the strength of a welded stud specimen spaced 18 inches on center. The connection was 4 times stronger in shear than the same connection without post tensioning. In flexure the connection held just over 2.6 times the moment that the welded stud connection held and cracked at 2.4 times the load that cracked the welded stud connection. Additionally, this is

the only connection type currently allowed in negative moment regions by UDOT. Despite these advantages, this connection type has problems with creep reducing post-tensioning forces.

Testing showed that the new curved bolt connection is an effective way to post tension a connection. The longer connection had 1.7 times the flexural capacity of the shorter connection. It failed at 1.2 times the moment required to fail the post tensioned connection and cracked at 0.8 times the post tensioned connection's cracking moment. While this connection was stronger than the post tensioned connection, it is believed that this is due to higher concrete strength in the curved bolt specimens. In reality the curve bolt connection strength would be slightly less than the post tensioned connection strength. The shorter curved bolt connection cracking moment was about the same as the welded stud connection or 0.4 times the post tensioned connection's cracking moment showing that the shorter curved bolt does not perform as well as the longer connection. Because the curved-bolt connections use significantly shorter rods than post tensioned connections do, this connection is expected to have significantly less compression loss due to creep compared to traditionally post-tensioned connections.

The welded rebar connection appears to be a better connection than the welded stud connection. UDOT should do a field study of bridges with this connection. Provided that the field behavior of this connection is good, UDOT should use it as a standard connection.

The curved bolt connection appears to be an effective way to post tension a bridge and a useful alternative to conventional post tensioning. UDOT should continue to study this connection. It needs to be tested to determine time effects (post tension losses, etc.) and the best geometry (bolt curve radii, bolt spacings, etc.).

1.0 INTRODUCTION

Precast concrete deck panels are becoming widely utilized for bridge deck replacements as well as new deck construction. Their importance is accentuated due to various departments of transportations' (DOTs) increased emphasis on accelerated bridge construction (ABC) techniques. Using precast panels allows bridges to be built faster as forming decks, tying rebar, and curing deck concrete can all be performed off-site. This significantly reduces construction times and traffic problems.

Precast bridge deck panels are placed on girders and connected by grouted pockets and rebar or Nelson studs to ensure composite action between the deck panels and girders. The panels then have to be connected to each other via panel-to-panel connections.

Despite the advantages with reduced traffic delays, transverse connections between precast bridge deck panels have experienced cracking problems in the field (Biswas et al. 1986; Issa et al. 1995a, b). Cracking allows water to leak through the panels and onto the girders below, leading to corrosion problems. Cracking can also damage asphalt and other overlays placed on top of the panels. Therefore, bridge engineers must consider speed and ease of construction, cost, and long-term performance when deciding to use precast deck panels.

In 2008, the Utah Department of Transportation (UDOT) developed standard specifications for precast bridge deck panels. UDOT was also interested in improving precast bridge deck connections and partnered with researchers at Utah State University (USU) to determine the service and ultimate shear and flexural strengths of five existing and proposed transverse connections. This research project provided laboratory testing of female-to-female precast bridge deck panel-to-panel connections. This was done to give UDOT a better understanding of the strengths and weaknesses of each connection as well as to discover valuable improvements to welded and post tensioned connections. With this information UDOT will be better able to choose the proper connection for a given bridge.

UDOT's standard welded stud and post tensioned connections were tested. The welded stud connection detail has a short life expectancy so a newly designed welded rebar connection was tested to determine if it can replace the current connection (UDOT 2008 b). The post tensioned connection uses conventionally post tensioning which works well but requires long rods that make it difficult to replace a single deck panel without replacing an entire bridge deck. The long rods or strands used in traditional post tensioning are also susceptible to creep and have problems with prestress losses. To provide an alternative to conventional post tensioning, two variations of a proposed curved bolt connection were tested to determine if they can provide post tensioning while at the same time allowing a single deck panel to be replaced. Connections were tested in shear and flexure. Deflections, cracking, and ultimate loads were recorded.

The purposes of this research project were to:

1. Determine shear and flexural strengths for all connections tested.
2. Determine what shear and flexural loads cause cracking in the various connections and the type of cracking.
3. Test female-to-female transverse panel connections under monotonic and cyclic loading.
4. Determine the feasibility of using a "curved-bolt" connection instead of conventional post tensioning.
5. Determine the benefit of using a welded rebar connection instead of a welded stud connection.
6. Give recommendations to improve connections and for further research.

This report begins with a review of relevant literature. Then a description of the connections tested, the test specimens' construction and testing apparatus setup are presented. Finally, results of shear testing (monotonic and cyclic) and flexural testing are presented. The results section includes load-deflection curves, a discussion of cracking, cracking photos, a discussion of capacities, and results from finite element computer analyses.

2.0 LITERATURE REVIEW

2.1 Deck Panel Connections

Connecting deck panels quickly and well is a challenge in bridges. The panels are usually connected to girders by small grouted pockets where Nelson studs or rebar loops extend from the girders into the deck panels to transfer the shear necessary for the deck panels and girders to act compositely. Deck panels also have to be connected to each other longitudinally (joint parallel to girders or running the length of the bridge) if the panels are not the full bridge width, and transversely (joint perpendicular to girders or running the width of the bridge). These connections can be done through closure pours, male-to-female joints or various female-to-female joints. They may be welded, post tensioned, or entirely unreinforced. This paper deals with transverse joints.

2.1.1 Closure pours

A closure pour is a type of reinforced joint made by splicing rebar between adjacent panels and then pouring concrete in between the panels. Closure pours are wider than other connections because they have to be wide enough to achieve proper development length in the spliced rebar. Because of this they tend to take longer to construct than other panel-to-panel connections. For this reason, many departments of transportation avoid them whenever possible. Connection widths can be reduced by hooking bars in the splice region (Brush 2004; Kim et al. 2003; Gordon and May 2006; Ryu et al. 2007).

2.1.2 Male-to-female connections

Male-to-female joints have been used for deck panel connections as well as in precast segmental bridge construction which uses precast sections with a continuous deck and girder. These connections are usually epoxied together. They are known to have problems due to stress concentrations from poor connection fitting (Issa et al. 1995b). Connections also have to be slid together, which can cause problems with the stud pockets used to attach panels to girders. Furthermore, the tight fitting of the connection does not provide any leeway for construction irregularities (Sullivan 2007). Because of the weaknesses in the male-to-female connection, it is not used very often in bridge deck panels anymore.

2.1.3 Female-to-female connections

Female-to-female joints have a grouted space between panels. Quick setting grout is used so construction time is minimal. The grouted pocket prevents the stress concentrations that male-to-female joints experience; however, because the joints are grouted it takes some time for the grout to gain strength before the bridge deck can be driven on (Yousif 1998). There are many variations of the female-to-female joint including unreinforced, welded, and post-tensioned connections.

2.1.3.1 Unreinforced connections

The simplest form of female-to-female deck joint is an unreinforced grouted keyway. Many bridges will have alternating lengths of unreinforced and reinforced keyway making up a transverse connection. Welded connections are usually done this way.

2.1.3.2 Welded connections

Welded female-to-female connections have plates cast into each panel. Once the panels are in place, a steel rod is generally placed between the plates of adjacent panels and welded on either side to the plates. The plates may be anchored into the concrete in many ways. The UDOT uses a welded stud connection with two Nelson studs welded to each plate. These studs go back into the concrete panel and anchor the connection (UDOT 2008a). Rebar has also occasionally been welded to the plates to anchor them (UDOT 2007). After the connections have been welded, grout is poured into the empty connection space (UDOT 2008a, b, c).

2.1.3.3 Connections with spliced reinforcement

Several systems have been developed to splice rebar similar to a closure pour, while maintaining a small, easily grouted female-to-female connection. The NUDECK system developed by researchers at The University of Nebraska-Lincoln uses rebar in pockets surrounded by spiral reinforcement to confine the grout and decrease longitudinal reinforcement development lengths (Badie et al. 1998a, b). Another method for reducing reinforcement development lengths was developed by The National Cooperative Highway Research Program

(NCHRP). They published a paper about splicing rebar in female-to-female connections using HSS segments to confine grout and decrease bar development lengths (Badie and Tadros 2008).

The NCHRP connection was recently adopted by UDOT as one of their standard connection details, called the shear key connection (UDOT 2008a). The NCHRP researchers performed lab testing on variations of this connection to determine preferred HSS sizes, bar lengths, etc. They also did full scale testing of a model bridge using this connection. The bridge was made by placing three deck panels on top of two girders. The panels were grouted to the girders. Then rebar was inserted in the transverse connections and grouted. The bridge was cyclically loaded in a low amplitude, high cycle fatigue test and shown to work well. This type of test has the bridge loaded at actual traffic loads over millions of cycles to represent fatigue. (Badie and Tadros 2008)

2.1.3.4 Post tensioned connections

Many female-to-female bridge joints have been post tensioned. The post tensioning helps to hold the connections together, keeps them in compression, and prevents cracking. For this reason, post tensioning is recommended by many researchers (Issa et al. 1995b; Yousif 1998) The NUDECK system mentioned previously has been used with post tensioning to improve bridge behavior (Fallaha et al. 2004). Post tensioned connections are preferred by UDOT for connecting panels due to their good field performance and ability to be used in negative moment regions (UDOT 2008b, c). Post tensioned connections require long rods or strands which make replacing a single deck panel difficult and also cause problems with creep leading to prestress losses.

2.2 Transverse Connection Field Performance

Several researchers have looked at field performance of connections. Biswas (1986) inspected a number of bridges with precast deck panels and found most to be performing satisfactorily. A few had problems and were leaking due to grout issues. One problem developed due to debris in the connection before grouting. This emphasizes the need to clean connections in the field before grouting. Another connection had problems due to a contractor's inexperience with a new grout.

Issa et al. (1995a) sent surveys to state departments of transportation about performance of existing bridges with deck panels. They also inspected existing bridges from 1993 to 1995 (Issa et al. 1995b). They found many bridges had cracking problems leading to corrosion of girders. Several male-to-female joints were found cracked and leaking. Problems were also found with non-post tensioned female-to-female connections. These connections had problems with cracking, leaking, and spalling of concrete. Welded connections also had cracking and leaking problems. Even several of the post tensioned connections were having problems; however, these problems were often attributed by the researchers to new materials. They concluded that several issues were causing connection problems. First, bridges that lacked post tensioning were having problems because the connections were not kept in compression and the joints were not tightened against leakage. They also discovered that some panels had problems because no gap between panels was provided to deal with dimensional irregularities in the field. Without the gap, stress concentrations formed where panels were in direct contact and cracking resulted. Yousif (1998) looked at bridges, including many of the same ones as Issa et al., and found similar problems.

2.3 Transverse Connection Lab Testing

To gain a better understanding of connection behavior, laboratory testing has been done by several researchers. These tests have been done on complete bridges and on smaller specimens. Tests may be full-scale or scaled down. Some directly test a connection’s shear, flexural, axial or other capacities while other tests instead try to mimic actual traffic loading.

Pure shear tests have been performed in a number of ways. One common way is by using a push off specimen constructed by connecting two “L” shaped specimens together to make an “S” shaped specimen. The resulting specimen is loaded on the top and bottom to place the joint in pure shear. Figure 1 shows push off shear specimens and how they are loaded. This type of setup has been used by many researchers (Bakhoum 1991; Issa et al. 2003).

Some shear tests have been done by connecting two sections of beams to form a beam like deck panel specimen. Kim et al. (2003) used this type of specimen to test connections in shear. They were also interested in the effects of post tensioning so they used two tendons to externally apply post tensioning to the panels. Strain gages were attached to the tendons to monitor the level of pre-stress applied to the connections. Figure 2 shows how the beam was loaded and restrained.

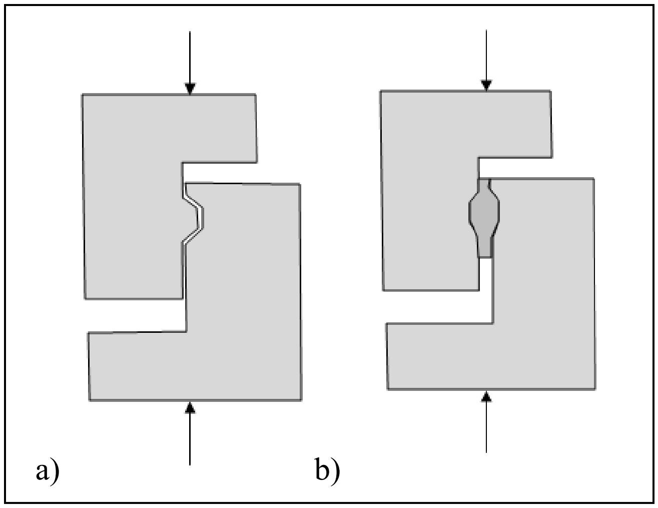

Figure 1. Typical shear push off test specimen designs.

a) Male-to-female connection, b) Female-to-female connection

The test specimens were fixed on one end and rotations were restrained on the other end. Then a distributed load was applied over a short distance from the rotation restrained end. This setup placed the joint in pure shear. The specimens were tested at different levels of pre-stressing. They were also tested cyclically at expected traffic loads for 2,000,000 cycles. Cracking in post tensioned connections was found to be through diagonal cracks. It was also found that pre-stressing increased fatigue strength, but even without pre-stressing the joints tested had enough strength to endure 2,000,000 cycles of load.

Because grouted joints or keyways have problems with leaking, Gulyas et al. (1995) looked at the grout materials used in precast concrete bridges. They found that in the field, cracks commonly form along the grouted keyways leading to leaking problems that increase corrosion of other bridge elements such as girders. They made small lab specimens 6 inches long with a grouted female-to-female connection in the center.

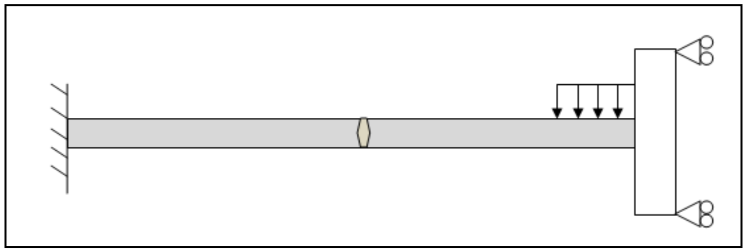

Figure 2. Shear test loading used by Kim et al. (2003).

The specimens were 9.5 to 12 inches deep and 3.25 inches wide. Various grout materials were used in the connections and tested to see which worked the best. These connections were then subjected to direct vertical shear, direct tension, and a loading similar to differential shrinkage, creep, or temperature movement. For the direct shear tests, one side of a connection was supported while the other end hung over an edge. Then a load was applied along the connection to shear it. This setup placed the connection in almost pure shear. Gulyas discovered that grout type, connection roughness and surface preparation all affect the strength of these connections. Issa et al. (2003) also studied the effects of grout on connection strength.

Flexural or moment testing of connections has also been done in numerous ways. Commonly a section of deck panel is simulated by connecting two concrete beams with a transverse connection in the middle. Then this beam is loaded to produce moment. Issa et al. (2003) used an 18 inch long flexural specimen to test grout strengths. The specimen was on simple supports and then loaded at the third points to produce pure moment in the connection region. Other researchers have chosen to use longer specimens, allowing for larger moments with smaller applied forces. Many researchers placed specimens on two simple supports with two equal loads spaced the same distance from each support. This type of loading places the connection in pure moment between the load points. (Brush 2004; Shim et al. 2005; Ryu et al. 2007)

Researchers at the University of Wisconsin have tested transverse and longitudinal joints in flexure. Their test setup had two panels connected by a transverse connection. The connection was at the midspan of the resulting beam specimen. Load was applied at the joint (midspan) and continued until failure. This loaded only the middle of the connections in pure moment. (Markowski 2005; Oliva et al. 2007).

Some researchers have tested specimens in negative moment. These tests are often done with a beam representing the panel with the connection in the middle. This beam is then placed on two simple supports with overhangs on either side. When loads act down on the overhangs, the connection at the midspan is placed in negative moment (Brush 2004).

Tension or pullout tests on specimens have been used to determine joint tensile capacity and rebar pullout strengths for connections. These tests have a specimen with a connection in the middle. This specimen is then pulled on the ends until failure in pure tension (Badie and Tadros 2008; Gordon and May 2006; Issa et al. 2003).

Other researchers have chosen to test bridge connections by building bridges and placing simulated traffic loads on them. These tests have at least two girders and several deck panels attached to the girders. Loads can be placed anywhere on the deck panels but are usually made to represent tire footprints to simulate traffic loads. Some researchers have used these tests with a single connection type, while others have built bridges with several different transverse connections. Building full bridges allows researchers to see how the different bridge elements interact and discover how the bridges react to actual traffic loading. The bridges are often tested for fatigue under traffic loads over millions of cycles of loading. Using girders and deck panels together also allows for composite effects between the beams and girders. In composite bridges the neutral axis will not be at the center of the deck so representing just the deck can misrepresent some of the bridge behavior. This type of testing does not allow researchers to test connections in pure shear, flexure, etc. and makes the results dependant on the girders used. These tests have been performed on scaled down models (Biswas 1986; Yousif 1998) and on full scale bridges (Badie et al. 1998a; Badie and Tadros 2008; Sullivan 2007; Yamane et al. 1998).

Full scale complete bridge testing also allows researchers to test for leakage. Sullivan (2007) tested connections during and after loading by ponding water on them and seeing if the water seeped through the connections. He found that post tensioned grouted female-to-female joints performed very well in durability testing. He also concluded that the post tensioned transverse connections he studied (male-to-female and female-to-female) all had enough flexural capacity. The connection types mainly differed in constructability and durability (cracking and leaking problems).

2.4 Finite Element Modeling

Finite element modeling is important in the study of precast concrete deck connections as it aids in evaluating results obtained from laboratory testing. If cracking can be represented in finite element analysis it would aid and simplify the studies of precast concrete bridge connections. An accurate working finite element model also allows for a larger range of analysis without the need of constructing physical specimens.

Different finite element models have been developed to confirm results from tested material. One common program for testing precast concrete bridges is ANSYS because of its built-in concrete capabilities and ability to perform nonlinear analysis. This aids in finding the initial cracking loads, and the location of these cracks.

Research done by Kachlakev, Miller, Yim (2001) on fiber reinforced polymer (FRP) retrofitted beams compared tested results to both linear and nonlinear finite element models. Two finite element programs that were used were SAP2000 (Computers and Structures, 1998) and ANSYS. The result shows that even in the linear range of the test ANSYS was closer to the test data than was SAP2000. This study tested both a control specimen and an existing bridge retrofitted with FRP laminates. The control specimen was tested to verify the efficacy of the finite element analysis. Then the bridge was modeled and compared with the test results from the existing bridge. The results indicated that the finite element model was stiffer than the existing bridge because of minor differences in material strengths and boundary conditions.

In a study performed by Bakhoum (1991), shear behavior between male-to-female connections were tested and compared with a finite element model. Several connections were modeled using ADINA (ADINA, 1986) finite element software which is able to model nonlinearity in different materials and the interface between them. This study is very helpful toward the process of finite element modeling. Both linear and nonlinear analysis were performed for the connection. The analysis included a model of the central part of the shear specimen, and a model of the entire shear specimen. It was determined that the entire specimen should be modeled when performing the shear analysis in order to obtain accurate results. The boundary conditions must also be well defined, or the results may be skewed. The model using linear analysis was approximately two times stiffer than the tested specimen. The nonlinear model increased the accuracy, but the first nonlinear model created did not give an accurate failure load. This was not obtained until accurate material parameters were entered, and proper strain softening and shear transfer coefficients were considered. The recorded deflections were applied to the model instead of applying loads. This was done to produce more accurate linear results. In this study Bakhoum stated that material failure envelopes are used to “establish uniaxial stress strain laws accounting for multiaxial stress conditions”, and to indicate whether cracking or crushing has occurred.

Research by Issa et al. (1995a,b; Issa, Yousif, and Issa 1995; 2003) was performed on grouted female-to-female shear keyway connections. Issa tested different shapes of shear keyways, and found that the connection with 1-1/4” gap at the top and 1/2” gap at the bottom had the least amount of cracking in the connection. It was also suggested that post tensioning be applied to allow for proper sealing between the connections. A finite element model was developed in ANSYS using SOLID65 elements which are able to model cracking and crushing of the grout. The analysis of the female-to-female shear keyway showed the major stress concentrations located in the grouting material along the connection joint and not in the concrete material. The model experienced cracking at the lower neck, and crushing at the upper neck of the model, with minor cracks in the concrete. The stress distributions across the connections were similar to the tested stresses, but the ultimate stress which occurred in the narrow neck of the connection had much higher stresses.

Sullivan (2007) analyzed transverse connections linearly in the finite element program SAP2000, and obtained nodal displacements and rotations. These values were then applied to the finite element model in ANSYS. This method of loading was similar to the method used by Bakhoum (1991). The loads were applied this way so that the analysis would be controlled by displacement rather than by an applied force which allowed for better convergence in the model. This study also used SOLID65 elements to model the concrete, but in places of irregular geometry SOLID45 elements were used. These elements were at the location of the connection, and did not have cracking capabilities.

THIS PAGE INTENTIONALLY LEFT BLANK

3.0 RESEARCH METHODS

3.1 Transverse Connections Chosen for Testing

UDOT developed standard specifications for precast bridge deck panels in 2008. The three standard connections are a post tensioned connection, a welded stud connection, and a shear key connection (UDOT 2008a). The latter was developed and lab tested in Report 584 of the National Cooperative Highway Research Program (Badie and Tadros 2008). Because the NCHRP connection had already been tested, UDOT asked that it not be tested for this project. The other two UDOT standard connections were chosen for testing to better understand how they behave and to provide a comparison with the new connections tested. Several other connections were also tested.

Figure 3 shows drawings of the welded connections tested. The welded stud connection is UDOT's standard welded connection. It has a six inch wide connection spaced one to two feet center to center. This connection also has known cracking problems and a short life expectancy. A welded rebar connection was tested as an alternative to the welded stud connection. It is very similar to the welded stud connection except it has rebar welded to the plates extending into the concrete panel as a way to anchor the connection. It has been used in a recent UDOT bridge on I84 in Weber Canyon (UDOT 2007). Testing this connection allows UDOT to know if their welded connection can be improved. The space between welded portions for both connections is also shown in Figure 3. These portions are unreinforced and only grouted.

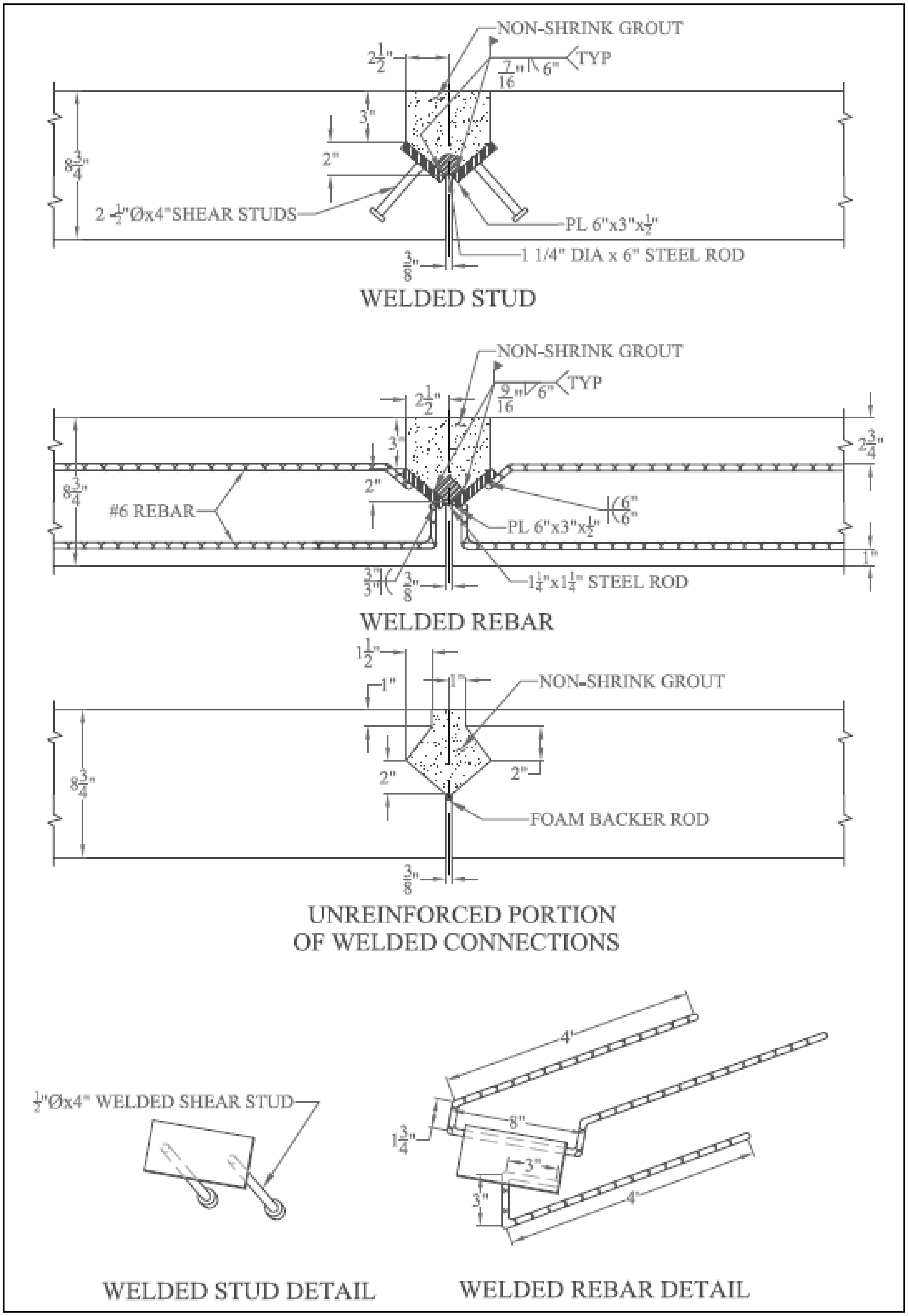

Figure 3. Welded connection details.

Figure 4 shows connections with post tensioning. The Post Tensioned connection is UDOT's standard post tensioned connection. It has post tensioning rods spaced at a maximum of every six feet. The rods run through ducts in the panels. They are tightened to provide 300 psi of post tensioning along the entire connection (UDOT 2008a). Two proposed variations of a curved bolt connection were also tested as part of this research. They are also shown in Figure 4. The proposed connections are based on a curved bolt connection concept used to connect precast concrete tunnel liners at the top of tunnels. Two bolt curve radii were tested making the connections 24 inches and 36 inches long. Both variations have curved bolts running through oversized ducts (1 ½ inch diameter) in the panels. After the connection area was grouted and set, the bolts were tightened to apply an average of 300 psi of horizontal pressure along the entire connection. In the flexural test specimens, two bolts were placed every 18 inches. The 24-inch long connection had two 1 inch diameter bolts while the 36-inch long connection had 2 7/8 inch diameter bolts. The ducts were not grouted in any of the specimens.

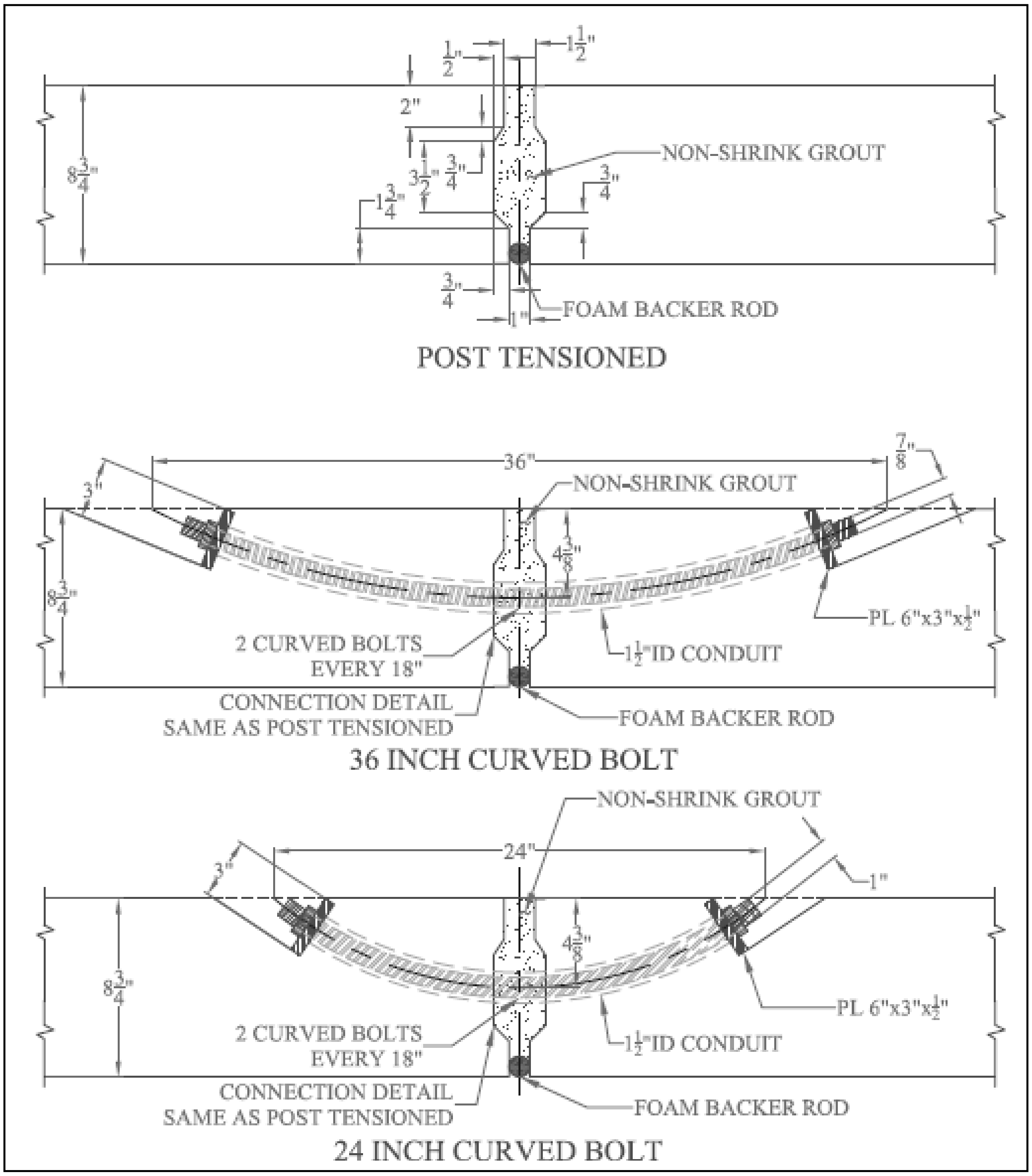

Figure 4. Post tensioned and curved bolt connection details.

3.2 Test Specimen Details

3.2.1 Shear test specimen details

For the shear tests, the connections were simulated using two L shaped concrete sections similar to those shown previously in Figure 1. These sections were then welded together (if applicable) and grouted together to form a shear specimen. This setup was chosen because it has been used by many previous researchers and loads a connection in pure shear (Bakhoum 1991;

Biswas 1989; Issa et al. 2003). The resulting specimen was six inches wide. This width was chosen because it is the length of the welded portion of the welded connections. The area between the welded plates was represented by another six inch wide specimen with just the unreinforced grouted diamond shaped connection that is between plates in the welded connections. Post tensioned connections were made using the grouted space between panels for the connection. No post tensioning ducts ran through the specimens. Instead, post tensioning was simulated by placing two pieces of channel iron on the sides of the specimen during testing and connecting them with four threaded rods. The rods were tightened and the strains in the rods measured. The rods were tightened to a strain that corresponded to a post tensioning force calculated to provide 300 psi of longitudinal compression over the transverse connection. Some samples of this connection were tested with post tensioning and others without. This was done to show the effect of post tensioning.

Shear specimen halves were reinforced with two layers of #3 bars to avoid failure away from the connection as suggested by previous researchers (Biswas 1989; Issa et al. 2003). Figure 5 shows a picture of this reinforcement in forms for a post tensioned shear specimen. Despite adding this extra reinforcement, some failures occurred away from the connection (the "arm") meaning more rebar was needed.

The test specimens were different from those used by other researchers because two pockets were left open in the specimens allowing them to fail more realistically. Figure 6 shows these pockets on a post tensioned shear specimen before grouting. The pockets are the empty spaces circled in the picture. These pockets allowed a 45-degree crack to form in shear and move through the deck portion without meeting the "arm" portion of the specimen. This also allowed the Nelson studs to pull out of the welded stud connections without being restrained by the specimen arm below them. During testing, cracking and other behavior was observed that would have been prevented by not including the pockets. Figure 6 also shows the "arm" portion of the specimens. They are the areas shaded with a grid.

Figure 5. Shear specimen form with reinforcement.

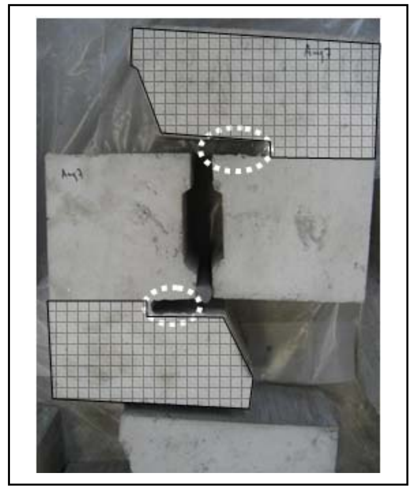

Figure 6. Post tensioned shear specimens before grouting.

(Shaded: arms or flanges, circled: pockets)

3.2.2 Flexural specimen details

Flexural specimens were made by grouting two beam halves together. Each half was 3 feet long, 18 inches wide and 8 ¾ inches deep, the standard panel depth specified by UDOT (UDOT 2008a). One side had a connection detail cast into the concrete. The welded connections had the six inch welded portion in the center with six inches of unreinforced connection on either side. The two specimen halves were connected by welding (if applicable) and grouting to form a single six foot long specimen. Specimens were reinforced with number 6 reinforcing bars in the configuration recommended in UDOT's standard specification manual. This configuration had two bars on the bottom of the panel and two on the top of the panel running perpendicular to the connection.

Bars were also placed parallel to the connection. These were number 6 bars hooked on both ends spaced at 3 inches on center (UDOT 2008a). Figure 7 shows the rebar setup. The curved bolt connections had curved conduits made of 1 ½ inch flexible pipe cast into the decks to provide a place for the curved bolts. Rebar loops were placed around the conduits for added reinforcement. No post tensioning rods or ducts ran through the post tensioned connection specimens. Instead, channel sections were placed on the ends of the specimens and connected with rods. Strains in the rods were monitored. The rods were tightened until the strains in the rods indicated that they had developed a force calculated to provide 300 psi of longitudinal compressive stress along the entire transverse connection.

Figure 7. Moment specimen reinforcement.

(Left: being tied, middle: In forms, right: curved bolt conduits and reinforcement)

3.3 Test Specimen Construction

To cast the shear and flexural specimens, plywood forms were built. The welded stud and rebar connections had the Nelson studs and rebar respectively welded to the plates by Bowman and Kemp in Ogden, Utah. Bowman and Kemp also cut and bent all the reinforcement for this project. The rebar was tied together at USU and inserted into the forms. Plastic spacers were placed on the rebar to ensure that one inch of clear cover was maintained between the rebar and the forms or floor to satisfy UDOT's specifications (UDOT 2008a).

Deck panel concrete was chosen to match UDOT specifications. It was an AA/AE mix with minimum f'_c of 4000 psi and a corrosion inhibitor admixture. The concrete was ordered from LeGrande Johnson in Logan, Utah and cast on three separate days. It was vibrated to ensure consolidation. 4 X 8 inch cylinders were made of each batch and tested at 28 days to determine the f'_c for each batch. Cylinders were also tested for tensile strength. The results of these tests are shown in Table 10 in the Appendix. The concrete was allowed to cure for one day before stripping the forms. Then wet burlap and plastic covering was placed on top of the specimens to keep them moist during curing.

After the specimen halves were cast and cured, two halves were placed together for welding (if applicable) and grouting. The welded stud connections had a 6 inch length of 1 ¼ inch diameter steel rod placed between the plates and then welded along the entire length as specified in Figure 3. Similarly, the welded rebar connection had a 6 inch length of 1 ¼ inch square rod welded between the two plates. Weld details were shown previously in Figure 3. During welding one of the welded stud shear specimens developed a small crack along where the Nelson studs ran through the specimen. This is theorized to have been caused from thermal expansion of the Nelson studs as the connection was welded. This was noticed early on in the welding. Future welds were allowed to cool before adding more weld material, preventing any cracking problems in subsequent connections. The specimen that cracked was used to test the shear test setup. While testing the setup, several problems with the setup were discovered and no results from the cracked specimen were used.

Threaded NC B7 rod was used to make the curved bolts for the curved bolt connections. This rod was tested at USU and found to have a yield stress of about 120 ksi. A machine was constructed at USU to bend the rods into the required curvatures. Figure 8 shows the bender used. This machine was made of ½ inch thick steel plates cut to the bolt curvature. A rod was inserted into this machine and the top plate of the machine was pressed down to bend the rod into an arc.

After bending, the curved bolts had the threads ground off of the middle of the bolts so that a strain gage could be applied to the bolt. Foil strain gages were applied to the middle of the center of the curved bolts to measure strains in the bolts so that the horizontal force in the bolts at the connection could be determined. In this way, the post tensioning of the curved bolts was determined. Figure 9 shows the curved bolts with applied strain gages.

After the curved bolts were inserted into the conduits, the ducts on either side of the connection were spliced. Figure 10 shows the curved bolt conduits after splicing. First, pipe insulation was placed around the bolt and slightly into each duct. Then, duct tape was wrapped around the ducts and insulation to seal the ducts and prevent grout from getting to the bolts or strain gages. Wires ran through the middle of the connection, coming out of the grout at the sides.

Before grouting, all connections were vacuumed with a shop vacuum and then power washed and dried. On the day of grouting the connections were wetted and kept damp for several hours before grouting to ensure that the concrete did not pull water from the grout.

The connections were grouted with Masterflow 928 non-shrink grout. This mix was chosen by UDOT because it is a commonly used grout for UDOT bridges. It is supposed to have a 1 day f'c of 5000 psi. Fibromac synthetic fiber reinforcement meeting UDOT specs was added to all grout batches. Batches of grout were mixed in the USU concrete lab. The grout was poured into the connections and prodded to ensure consolidation. Then 1100-CLEAR curing compound was sprayed on top of the grout to satisfy UDOT specs. Cylinders were made to determine the 1 day compressive strength of the grout. Results of cylinder compressive tests are shown in Table 11 in the Appendix. Because the initial strength of all cylinders did not reach 5000 psi within 24 hours, additional cylinders were tested at 48 or 72 hours to ensure the 5000 psi strength was developed before the connections were tested. All cylinders gained the required 5000 psi strength. The welded shear specimens were not prodded and holes developed in the grouted pockets. These were later patched with new grout.

Figure 8. Threaded rod bender.

Figure 9. Curved bolts with strain gages.

Figure 10. Curved bolt conduit splicing.

3.4 Finite Element Modeling Properties

The finite element program ANSYS 11 was used to create and analyze models of all the tested connections. This software was chosen because of its capacity to model cracking in concrete. Models were developed for both shear and moment testing, and load deflection and moment deflection curves were plotted for comparison with the laboratory testing.

The material properties for the elements used in this analysis are defined by four different categories: element type, real constant, material model, and key options. The element types for the models are SOLID65, SOLID45, and LINK8. Real constants are inputs that describe the geometry for LINK8 elements and rebar specifications for SOLID65 element. Material models are the linear and nonlinear properties that define the elements' behavior. The material models used in this research were linear, bilinear isotropic hardening, and the built in material model for concrete. Key options (KEYOPT) inputs determine whether to include or disable certain element functions. Default KEYOPTs are used for all the elements except SOLID65 and contact elements. Each element will be described with its corresponding real constants and material models in the following paragraphs.

LINK8 elements are line elements with three translational degrees of freedom. These were used to model the steel plate, welded rebar, shear studs, and other rebar reinforcement within the panel. The real constant input for a LINK8 element is the cross sectional area. Linear and nonlinear material models were used for the LINK8 element. The linear model properties are the modulus of elasticity (E) and Poisson's ratio (ν). These values for steel are E = 29,000,000 psi and ν = 0.2. Bilinear isotropic hardening was the model used to simulate yielding in the steel, and had a yielding stress (f_y) of 60,000 psi, and a tangential modulus of elasticity (E_t) of 2,900 psi. The modulus and yielding stress are in accordance with UDOT's specifications for structural steel for these connections.

SOLID45 components are eight node 3D elements with three translational degrees of freedom. In this research these elements act as bearing plates to reduce major stress concentrations in the models at the loading and bearing points. SOLID45 elements do not have a real constant, and has the same linear material properties as the LINK8 element (E = 29,000,000 psi, ν = 0.2). These plates are used for modeling purposes, and are not representative of physical plates used during laboratory testing.

SOLID65 elements are eight node 3D solid elements with three translational degrees of freedom at each node, and are used to model the concrete and grout. The real constant for a SOLID65 element indicate the material, volume ratio, and direction of reinforcement in the element. As opposed to using a line element to model rebar in discrete locations, a built in reinforcement option, known as smeared reinforcement was used. This method was implemented to simplify the modeling of reinforcement in the panel. The material for the smeared reinforcement is input by using the predefined material model number. The volume ratio is the ratio of the reinforcement volume over the total element volume (ANSYS, 2007). The direction of the reinforcement is indicated by two angles (θ and φ). The angle θ is measured from the X to the Y axis, and φ is the angle to the Z axis. The real constant for the SOLID65 element has the option of reinforcement in three different directions, but in this analysis only the Y and Z direction were used. Reinforcement in the X direction was omitted to avoid having the reinforcement acting at the connection.

Both linear and nonlinear material models were used for SOLID65 elements. The linear properties include the modulus of elasticity (E_c) and Poisson's ratio (ν). The modulus of elasticity for concrete and grout was calculated using the following equation:

$$E_c = 57000\sqrt{f'_c}$$

where f'_c is the uniaxial compressive stress and values for the concrete and grout are 4,000 psi, and 6,000 psi, respectively. These values are the specified compressive strength for concrete used in ABC, and three day compressive strength indicated by the grout manufacturers. The Poisson's ratio for each was taken as 0.3.

The nonlinear material model used for SOLID65 elements was the concrete model which predicts the failure of brittle materials. A failure surface is defined by five different stress parameters: uniaxial tensile cracking stress (f_t), uniaxial compressive stress (f_c'), biaxial compressive stress (f_{cb}), ambient hydrostatic stress state (σ_h), biaxial crushing stress under the ambient hydrostatic stress state (f_1), and uniaxial crushing stress under the hydrostatic stress state (f_2).

Concrete tensile tests were performed on cylinders made from the concrete used in the specimens, resulting in an average tensile strength of 480 psi. Because of convergence problems in ANSYS, the crushing feature was turned off using a value of -1. This was done to save computational time and focus on the cracking that occurs within the specimens. Crushing has been turned off in other studies because it was problematic towards obtaining an accurate solution (Kachlakev, Miller, and Yim, 2001; Wolanski, 2004). By doing this, the material cracks whenever the principle stress component is higher than the tensile stress of the concrete and the remaining parameters (f_{cb}, f_1, and f_2) are suppressed (ANSYS, 2007).

Three other inputs for the concrete model are shear transfer coefficient for open cracks (β_t), shear transfer coefficient for closed cracks (β_c), and stiffness multiplier for cracked tensile condition (v^1_r). Shear transfer coefficients range from values of 0.0 to 1.0 with 0.0 representing a smooth crack with no shear transfer, and 1.0 representing a rough crack that transfers the entire shear. For this analysis β_t was set to 0.2 representing a fairly smooth crack, and β_c was set to 0.6 representing a moderately rough crack. A value of 0.2 was suggested in Wolanski (2004) because when β_t for an open crack drops below 0.2 convergence is difficult to achieve. The value of the stiffness multiplier for cracked tensile condition was taken as the default value v^1_r=0.6.

KEYOPTs are used in SOLID65 elements to help solution convergence. KEYOPTs are different for each element, and for the SOLID65 elements key option (7) is used to help convergence when the element is undergoing cracking. KEYOPT(7) was set to a value of 1 which gives the option to include tensile stress relaxation after cracking. When a crack occurs in an analysis the stress available at that node drops to zero, which often causes convergence problems. Stress relaxation allows for a more gradual reduction helping in obtaining a converged solution.

Initially the concrete to grout contact was modeled as continuous, but analysis showed that the concrete separating from the grout had a significant impact in the force deflection curve. In order to model the bond and separation of the concrete and grout contact pairs with debonding capabilities were implemented. Contact pairs consist of two elements: a target element (TARGE170) and a contact element (CONTA173). These elements define the boundary between the surfaces of the concrete and grout, and have the ability to model delamination of the two surfaces. The TARGE170 elements overlay a 3D solid element and characterize the boundary conditions. These are associated with the contact elements by sharing a real constant set. The CONTA173 element is able to model surface to surface contact between 3D solid elements. The stiffness between the surface and target can be modified to define the bond characteristics.

The real set constants for contact pairs have the option of 26 inputs, however, only one of these inputs were changed from the default settings. Initial analysis of each model without using contact pairs had a linear region before cracking that was far more rigid than the tested specimens. This suggests that there is some softening in this initial region. To imitate this initial softening, the normal penalty stiffness factor (FKN) was reduced.

CONTA173 elements have twelve key options available, and five were changed from their default values (2,5,9,10,12). KEYOPT(12) indicates the initial bond behavior of the contact pairs. In this analysis the bond is represented as fully bonded by setting KEYOPT(12) to 5, and the separation is modeled using a cohesive zone material model. KEYOPT(2) controls the contact algorithm, which was changed to the penalty method as suggested when KEYOPT(12) is changed to a value of 5. The penalty method is a contact algorithm which defines the stiffness between the two surfaces as a spring whose stiffness is equal to the FKN value (ANSYS, 2007). The stiffness was updated after each iteration by changing KEYOPT(10) to a value of 2. While constructing the model an initial gap was found between the concrete and grout. This gap was insignificant, but potentially detrimental to the analysis. Using KEYOPT(9) and (5) equal to 1 the initial gap was neglected.

In order to allow for separation between the grout and the concrete a Cohesive Zone Material Model (CZM) was used. This works by a constitutive relationship between the traction on the interface, and the corresponding separation across the interface (ANSYS, 2007). The bond between the concrete and grout was defined by using the real constant for the contact pairs, and the CZM material model inputs.

The CZM model has bilinear behavior by using one of two set options; traction and maximum separation, or traction and release energy. In this analysis the traction and maximum separation was used which has 6 input option; maximum normal contact stress (σ_{max}), contact gap at the completion of bonding ($u^c{}_n$), maximum tangential stress (τ_{max}), tangential slip at the completion of bonding ($u^c{}_t$), artificial damping coefficient (η), and an option indicator for tangential slip under compressive normal contact stress (β). Because sliding does not control the separation only σ_{max} and $u^c{}_n$ were used in the CZM. The artificial damping is included to compensate for convergence problems that are caused by modeling debonding. The damping input has units of time and is multiplied by the smallest time increment. ANSYS suggests the value be between .1 and .01; in this analysis the value was taken as the minimum suggested value of .01 for all the models.

A static analysis was performed for each of the models and a full Newton-Raphson method was used for the nonlinear analysis. The load was divided into multiple substeps until the final load was achieved. The load step increment was chosen by ANSYS, so if the solution was not converging at a certain load substep, the increment decreased until convergence was reached. The number of substeps was increased until a full analysis was reached for the load step. While developing different models, properties and meshes were changed, and some analyses would not converge. In order to exit an analysis that is not converging a maximum number of equilibrium equations was set. This number was set from 50 to 200 equations depending on the type of connection and model.

4.0 DATA COLLECTION

Laboratory testing consisted of shear and flexural testing. Shear specimens were loaded monotonically to failure and cyclically in high amplitude, low cycle tests. Flexural or moment specimens were loaded monotonically to failure. Table 1 shows the number of specimens tested for each connection in each type of test. Originally three specimens of each connection type were cast for each test type; however, in actual testing the number of specimens tested was adjusted to those in Table 1 due to problems encountered in testing and when more data points were desired for a given test.

Table 1. Quantities of Test Specimens Tested

Connection Type	Test Type		
	Monotonic Shear	Cyclic Shear	Flexure
Welded Stud	4	2	3
Welded Rebar	2	0	3
Unreinforced Portion for Welded Connections	4	2	0
Non Post Tensioned	2	1	0
Post Tensioned	3	4	4
24-inch Curved Bolt	0	0	3
36-inch Curved Bolt	0	0	3

4.1 Test Apparatus Setups

4.1.1 Shear test apparatus setup

A loading frame was used to test the shear specimens. The setup of this frame is shown in Figure 11. The shear specimens were placed on a six inch by six inch steel bearing plate centered on the connection. Another six inch square plate was placed on top of the specimen, also centered on the connection. A spherical head was placed on top of the plate to ensure that the load would be vertical even if the top of the sample was uneven. This setup loaded the connection in pure shear. A load cell was placed on top of the spherical head in order to measure the shear load applied to the sample. A beam ran from the load cell to two yokes attached to four rods which extended beneath the floor into hydraulic rams. These rams pulled down on the rods which transferred the load through the yokes and beam and into the specimen.

Initially a specimen was tested and found to rotate under load rather than fail vertically. To counteract this problem a harness made of channel sections and threaded rods was attached to all future specimens. This harness can be seen in Figure 11. It was not post tensioned. This made it so the samples would not rotate and made the panels behave closer to field conditions where many feet of panel effectively confines the connection and prevents large rotations. The harness could also pick up any moments caused by slight eccentricities in the loading. For the post tensioned connections, the harness was tightened to simulate post tensioning.

An LVDT device was used to measure deflections. The rod from the device rested on the top of the specimen in the corner. It was anticipated that this would show the relative displacement of the two segments of the connection as it failed. In some specimens the part of the specimen away from the deck experienced cracking. This cracking caused rotations and displacements away from the connection. This made the LVDT measurement somewhat unreliable. Despite this problem, large downward (positive in figures) deflections still show that failure has occurred.

The specimens were initially loaded to failure with at least three tests per connection type. In each test the load was gradually applied until failure. Before failure, cracking and the associated cracking loads were noted. The final failure method was also noted.

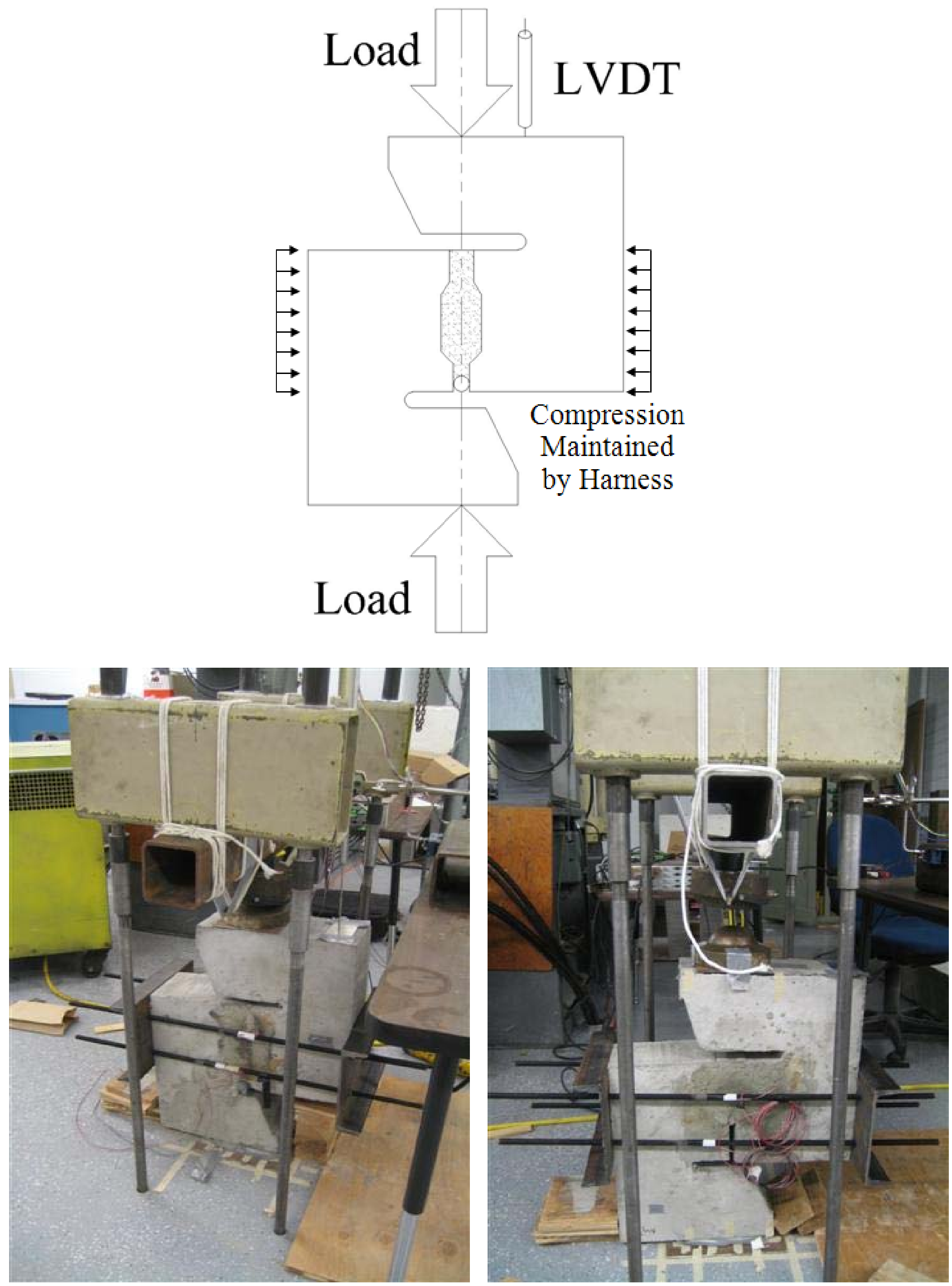

Figure 11. Shear test loading frame.

4.1.2 Flexural test apparatus setup

Flexural specimens were tested in the loading frame shown in Figure 12. The flexural specimen rested on two roller supports with two inches of overhang on each side. Two equal loads were applied one foot from each support. This setup placed most of the specimen, and all of the connection, in pure constant moment.

Some panels had a harness around them consisting of two channel sections and threaded rods. Strains were monitored in the rods to ensure that they were not picking up loads. The harness was in place to hold the panel together as it failed. The rods did not pick up any load until immediately at failure.

The post tensioned panels used a harness to apply post tensioning. Two rods ran between channel sections at the ends of the panels. Strain gages were applied to the rods. Then the nuts on the rods were tightened until the strains in the rods reached those required to apply 300 psi of compressive stress to the entire connection area. Similarly, the curved-bolt flexural connections were tested after the bolts were tightened to a stain that was calculated to apply 300 psi of horizontal stress over the entire connection.

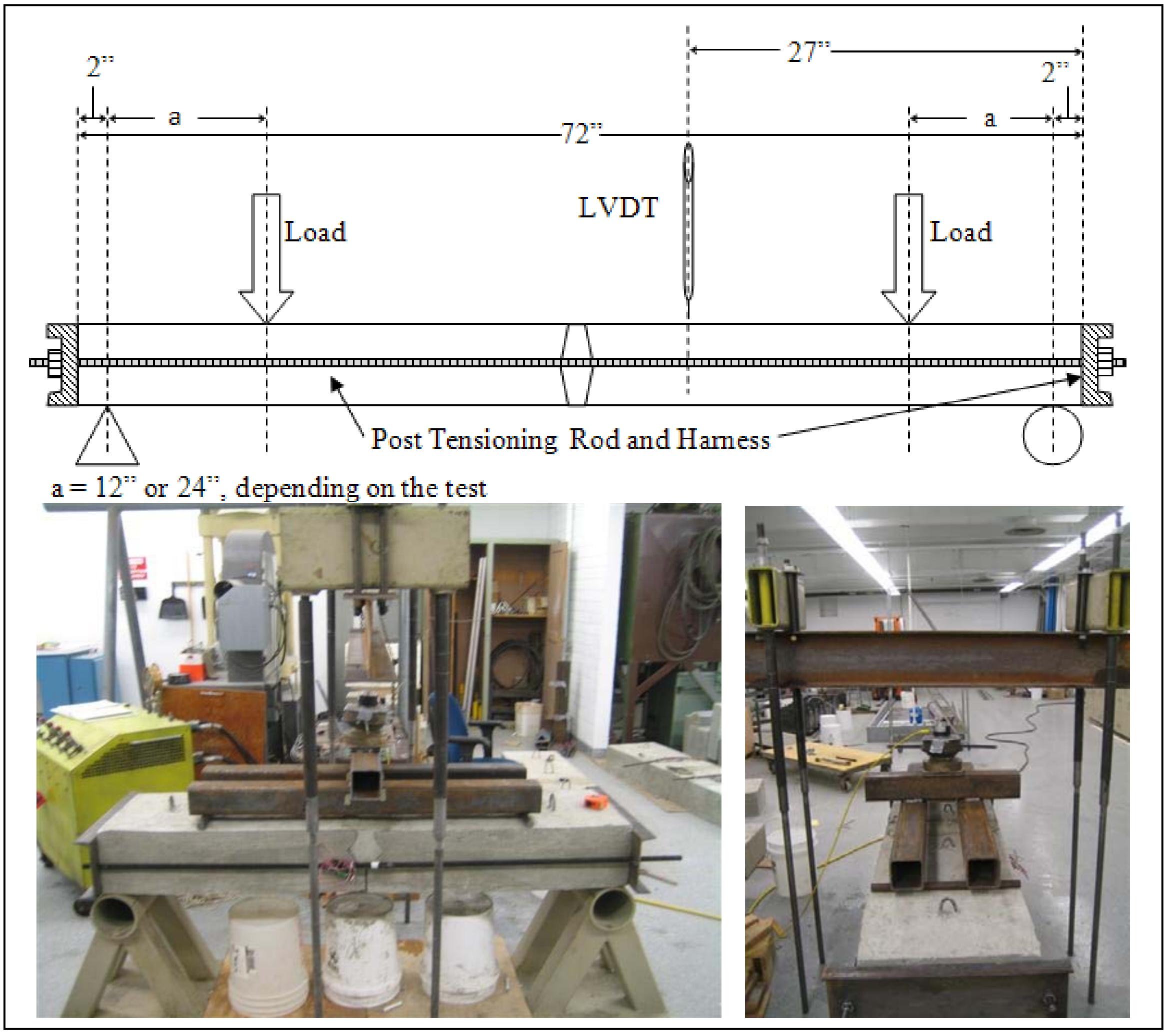

Figure 12. Flexural test loading frame.

Flexural specimens were loaded monotonically until failure. Cracking was recorded along with the corresponding cracking loads. Also, the manner of cracking was recorded. Vertical deflections of each specimen were measured 27 inches from the edge of the panel (25 inches from the support) using an LVDT. This distance was chosen because it allowed the LVDT to be near the panel center without interfering with other equipment.

The longer curved bolt connections (36-inch), post tensioned connections, and welded rebar connections were anticipated to hold more load than the loading frame was able to deliver. To overcome this problem, the loading points were moved to two feet from the supports to double the moment for a given load for these specimens. This still provided pure constant moment without shear in the connection area.

4.2 Setup of Finite Element Models

4.2.1 Shear Specimen Finite Element Modeling

In order to obtain a consistent mesh with the differing geometry, the order and creation of the finite element model and mesh were critical. The process is shown in Figure 13. The models were divided into a series of quadrilaterals with keypoints inserted at the corners of these areas as shown in Figure 13(a). From these keypoints a parallel plane of keypoints were generated, and solids were created between the two planes using the keypoints as shown in Figure 13(b,c). The individual solids were connected using the ANSYS Boolean Glue function, and adjacent lines and keyponts were combined into one. By doing this the individual solids are still able to maintain their different properties. All solids of one type were selected, and the corresponding properties were assigned before a volume was meshed.

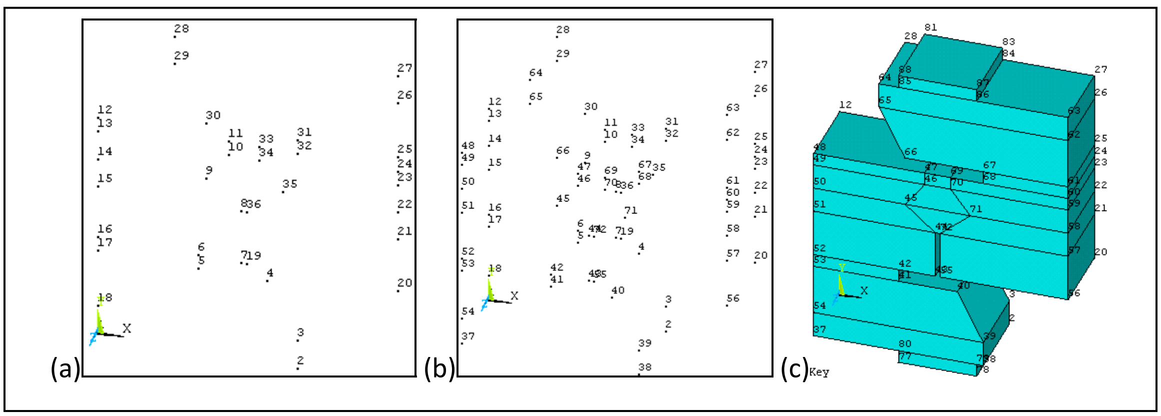

Figure 13. Shear model creation sequence.

To create line elements such as a shear stud, a line is selected from a volume, assigned the reinforcement properties, and meshed. Because of this process, the solids were divided in order to create boundaries where line elements could be assigned. The welded stud model has a plate on an angle with shear studs perpendicular to the plate. In order to create a boundary line where the stud was located, certain volumes were divided at angles creating geometry that is difficult to mesh. At these locations some triangular meshes were used. Triangular shapes are not recommended for use in SOLID65 elements, and are used only where no other option could be found.

The geometry for the shear models were the same as the geometry for the tested specimens. SOLID45 elements were used to model a 6” x 6” x 1” bearing plate located at the loading points, and centered over the connection. Figure 14 shows the steps in applying the boundary conditions. The bottom plate was fixed against translation in the Y direction (Figure 14 a), the right and left outside face of the model was fixed against translation in the X direction (Figure 14 b), and the back face of the model was fixed against translation in the Z direction (Figure 14 c). The load was applied to the top of the upper plate evenly distributed at the nodes (Figure 14 d).

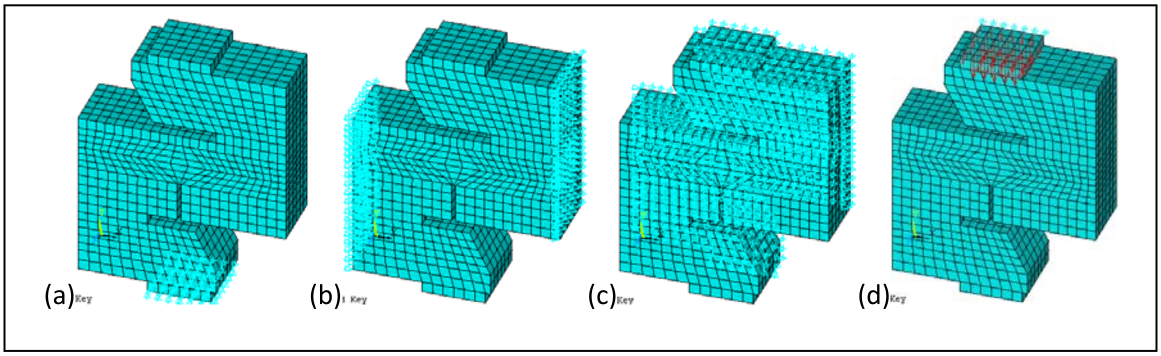

Figure 14. Shear model boundary conditions sequence.

The welded stud connection was created by using LINK8 elements for the steel plates and shear studs. The steel plate could not be modeled with a plate element because it has rotational degrees of freedom which would create inconsistencies along the

boundary of the solid elements which have only translational degrees of freedom. The cross sectional area for the line elements used to model the plates was 1.277 in^2 and the area for the welded studs were 0.2 in^2.

UDOT standards require post-tensioned connections to have at least 300 psi be applied across the face of the connection for adequate post tensioning (UDOT 2008c). In the post tensioned model, a horizontal pressure of 300 psi was applied to the outside left face of the model and an analysis was performed to ensure that 300 psi was acting across the face of the connection before the vertical load was applied.

Some properties in the models were changed in order to better model the behavior of the different connections. The concrete, grout, and steel properties were consistent for all the shear models. The properties changed were the variables affecting the contact behavior between the concrete and the grout which are, σ_{max}, u^c_n, and FKN. The value for σ_{max} is 480 psi, the same value as the tensile strength for the concrete. u^c_n was taken as 0.015 inches, representing a relatively small separation between the concrete and grout upon failure of the bond. The value for FKN that was used was 0.0011 for the shear specimens. This value is multiplied by the normal contact stiffness resulting in relatively low contact stiffness. During testing it was observed that the bond between the concrete and the grout was very weak, and separation often occurred along this boundary. Because of this weak bond the normal contact stiffness was reduced.

The applied load and deflection were recorded at each incremental loadstep. The nodal deflection was recorded in the center of the specimen one inch from the right edge on the top flange. This was the approximate location of the LVDT during the physical testing. Cracking sequences were also recorded for each connection. The four different models analyzed in shear are: 1) unreinforced portion of the welded tie, 2) welded stud, 3) non-post tensioned, and 4) post tensioned.

In ANSYS when the principle stress at an integration point in a concrete element exceeds the tensile stress, cracking occurs. This is modeled by an adjustment of the material properties and is called a "smeared crack" or region of cracking. Cracking is available in three orthogonal directions at each integration point which is indicated by a red (first crack), green (second crack), or blue (third crack) circle. The cracking represented from the finite element model is not a finite crack, but an area where cracking occurs. Cracking in multiple directions indicates considerable cracking, and is regarded as a location where visible cracking can occur. A more detailed description of the finite element predicted cracking sequence will be given for each connection.

Similar to the tested results, the finite element models also experience cracking in the flanges away from the connection. However, in the analysis, the arm did not fail, but continued to crack which did not result in cracking in the connection until very high loads (nearly double the ultimate load of the tested specimens). To better model the behavior of the specimens two options were modified. First, the concrete crushing and cracking capabilities were turned off for all the concrete that was part of the upper and lower flanges to better localize cracking in the connection. Second, contact pairs were used at the interface between the concrete and the grouted connection. These changes produced a behavior in the model that was similar to the tested model.

The result from the unreinforced portion of the welded tie connection is used to illustrate the accuracy gained from using contact pairs. After each analysis a force deflection curve was created using the applied load and deflection from each substep. The deflection was measured at the approximate location where the deflection was recorded during the laboratory testing. The finite element model without the contact pairs is approximately 21 times stiffer than the model with contact pairs. The force-deflection curve of the model with the contact pairs more accurately follows the approximate curve of the tested specimens.

4.2.2 Flexural Finite Element Modeling

The flexural models were created similar to the shear models – keypoints were created, solids were generated from those keyponts, and assigning and meshing of the solids was performed. However, due to symmetry, one quarter of the geometry was modeled in ANSYS, and proper boundary conditions were applied at the plane of symmetry. The specimen was divided lengthwise along the centerline and then fixed against movement in the X direction on that face. Likewise, the model was divided widthwise, and fixed against translation in the Z direction along the face of the divide as is shown in Figure 15. A 9” x 4” x 1” solid with steel properties was modeled at the loading and bearing points – on top of the beam 22 inches from the left hand side and at the bottom left corner – to avoid stress concentrations. The beam was modeled as simply supported by pinning the nodes along the center of the bearing plate in the Y direction. This was suggested by Kachlakev, Miller, and Yim (2001) to allow for rotation and avoid cracking in the concrete around the bearing plate. The load was distributed to the nodes along the center of the loading plate. The loading plate was moved 12 inches from the

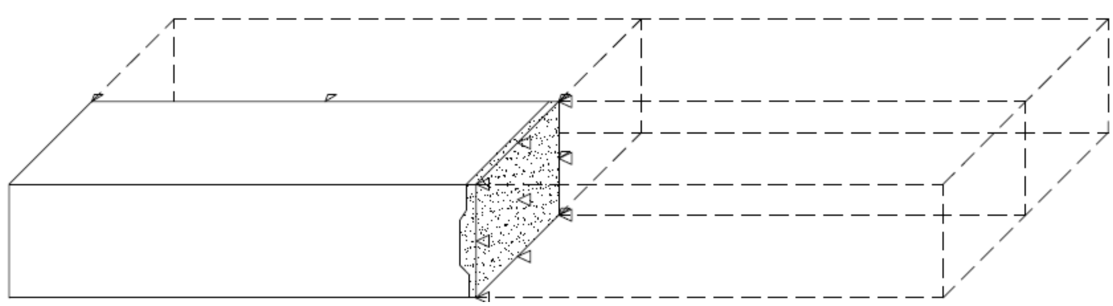

Figure 15. Quarter scale flexural model.

right side for the 24 inch curved bolt model because the 4 inch plate interfered with one end of the curved bolt. Because of the different geometry of each model, a uniform mesh could not be obtained, but a one inch element size was attempted for each model.

In order to model the post tensile force for the simple post tensioned models, a uniform pressure of 300 psi was applied over the area on the right end of the model. A test was run without applying a vertical force, and the stresses were analyzed to ensure that 300 psi was acting across the connection.

In the laboratory testing the curved bolt connection was made by bending threaded rods to a specific curvature and feeding that through oversized conduits across the connection. After the grout was placed steel plates with holes were placed on the ends of the rods and nuts were used to tighten the bolt to the post tensile force. This was modeled in ANSYS using LINK8 elements with steel properties for the curved bolts. The curved portion of the bolt was simplified as several linear elements, which were connected to the concrete and grout elements at specific nodes. The post tensioned force was modeled by applying a temperature differential across the curved bolt elements. A coefficient of thermal expansion of 12×10^{-6} in/K was used and temperatures were changed until an average stress of 300 psi was observed across the connection. In addition the strain was output for the curved bolt and compared to the strain obtained through laboratory testing, and final minor temperature adjustments were made to match the tested strain. For the 24 and 36 inch curved bolt the temperature difference was -115 K, and -130 K, respectively.

The contact pairs behave differently when used in shear dominated analysis and bending dominated analysis. Some of the contact inputs have been changed for this reason. The value for σ_{max} remained the same value as the tensile strength of the concrete (480 psi). Except for the welded stud connection, the value of u^c_n was kept at 0.015 inches. In this connection the contact gap affected the results significantly whereas the other connection showed little change. The welded stud had the best results when u^c_n was set at 0.016 inches. The value for FKN was changed to from 0.0011 to 0.0036 for the flexural specimens. Also the cracking coefficients β_t , and β_c for the welded rebar connection were changed from 0.2 and 0.6 to 0.9 and 0.9, respectively. Since little separation occurred between the grout and concrete in this connection the resultant cracks were very rough.

The ultimate load capacities for the laboratory tests were applied to the finite element models and analyses were performed. The load was recorded at each substep, and nodal deflections were obtained at a location 27 inches from the left side of the beam, as was performed during laboratory testing. Moment-deflection curves were created for each type of connection using these recorded deflections and loads. The five different connections that were modeled are: 1) post tensioned, 2) welded rebar, 3) welded stud, 4) 36 inch curved bolt, and 5) 24 inch curved bolt. Images of crack progression were captured for each of the models and compiled into figures. These figures show the grouted connection with approximately five inches on either side of the connection for the laboratory tested specimens. Because half of the specimen was modeled in the finite element analysis, the figures for the predicted cracking show only half of the specimen.

Similar to the shear models, contact pair elements were used to mimic the concrete to grout bond and add an initial softening that occurs in the tested specimens. Without the contact pairs the moment-deflection curve for the post tensioned connection resulted in an initial slope that was approximately 8 times larger than the tested results.

THIS PAGE INTENTIONALLY LEFT BLANK

5.0 DATA EVALUATION/ANALYSIS

5.1 Monotonic Shear Test Results

5.1.1 Shear specimen ultimate capacities

Shear specimens were tested monotonically in pure shear to failure. Information for each specimen, including concrete cast date, grout date, and testing date are found in Table 8 in the Appendix. Table 9 in the appendix provides a summary of the monotonic shear test results.

In the tables the ultimate capacity of the connections are for a six inch length of connection, the length of the shear specimens. The welded rebar connections are not included because they failed away from the connection, so shear strength was unable to be determined. Although the ultimate shear capacity of the welded rebar connection is unknown, the fact that it failed away from the connection implies that it has high shear strength. This is probably because for the connections to fail in shear the welds must fail or the rebar has to pull through the panels. With long pieces of rebar making up the connection, tearing through the panel becomes difficult.

Figures 16 through 19 show shear-deflection curves for the monotonic shear test specimens. In these figures deflections in inches are shown on the horizontal axis and shear load in lbs are shown on the vertical axis. Markers are also used in these figures to show where cracking was recorded. Results from the finite element models are also included on the figures.

Figure 16 shows the laboratory and finite element shear-deflection curves for the specimens representing the welded portions of the welded stud connection. These connections deflected more rapidly than the post tensioned connections, but they still withstood relatively high shear loads before reaching their ultimate capacities. In order for the welded stud connection to fail, the welds must fail or the studs have to pull out from the concrete. In the actual testing the Nelson studs pulling through the concrete was the ultimate failure mode as will be discussed later. These connections cracked at low loads. The finite element model for the welded stud connection followed the tests results except for one test which has a greater deflection. The points where there are loops in the curves are when cracking occurred away from the connection in the arm or flange which caused rotation in the specimen. This caused the LVDT to rise and fall rapidly, and does not have a correct correlation with the deflection occurring in the connection. The finite element model follows the tested results approximately until this point. Once major cracking occurs the modeled connection has a linear deflection.

Figure 17 shows the shear-deflection curves for the unreinforced specimens for welded connections. At low loads the grout-concrete interface separated and then these specimens experienced relatively large deflections. These specimens cracked and failed at relatively low loads. The finite element model for these specimens behaved similarly to the tested connections with separation in the concrete and grout in the upper left and lower right portions of the keyway. After this initial separation the deflection continued linearly until the ultimate load.

Figure 18 shows the shear-deflection curves for the post-tensioned type connections without applied compression. These specimens experienced more deflection than the same connection with post tensioning and failed at relatively low loads. The force-deflection curve for the non-post tensioned connection is fairly simple. The finite element model followed the curve of one specimen, but tends to be more rigid than laboratory testing indicated. Cracking occurs in the model at the point on the graph where the curve flattens out (approximately 7,400 lb). This agrees with the tested specimens where failure occurs immediately after cracking.

Figure 19 shows the shear-deflection curves for the post-tensioned type specimens with 300 psi of compression applied to the connection area. These specimens deflected the least for a given load of the connections tested. They also the highest ultimate capacities of the connections tested. The finite element analysis for the post tensioned connection closely follows the laboratory results with a similar trend in curvature.

Both the specimens representing unreinforced portions of the welded connections and the non-post tensioned connection specimens have low shear capacities. This is probably because neither connection is reinforced or post tensioned to add to shear strength. When post tensioning was applied, the post tensioned connection gained significant strength and was the strongest connection in shear.

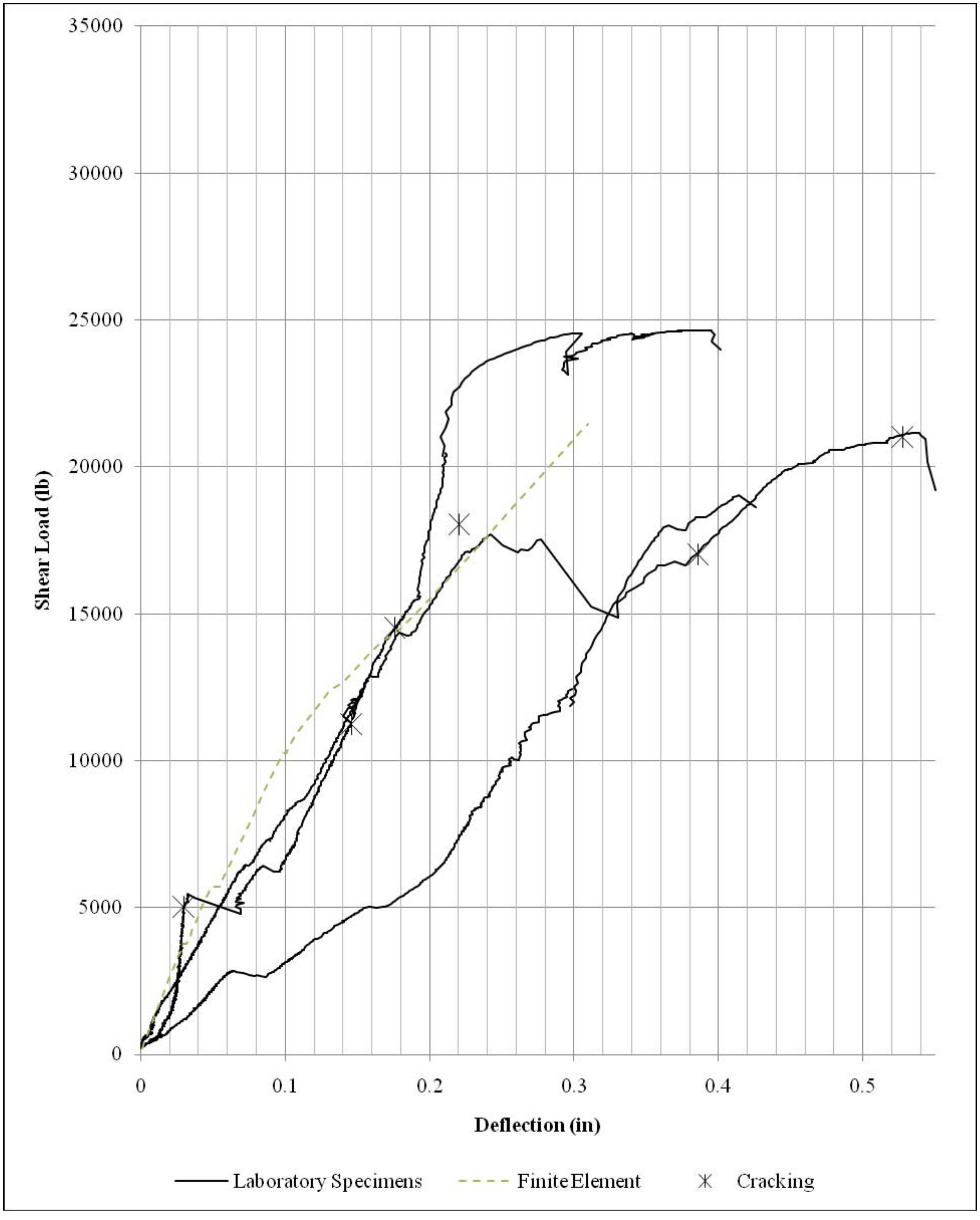

Figure 16. Shear-deflection curves for welded stud specimens.

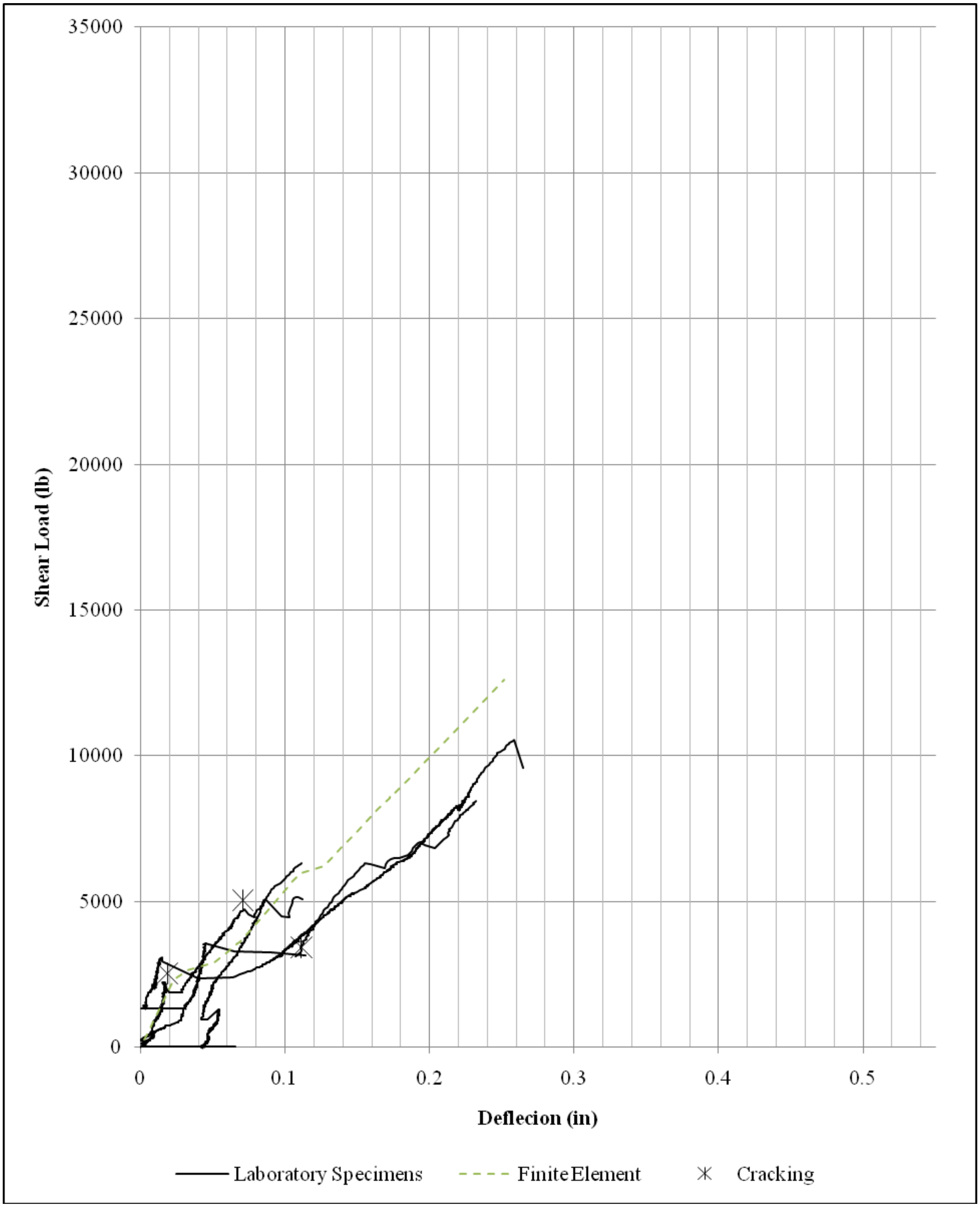

Figure 17. Shear-deflection curves for unreinforced specimens for welded connections.

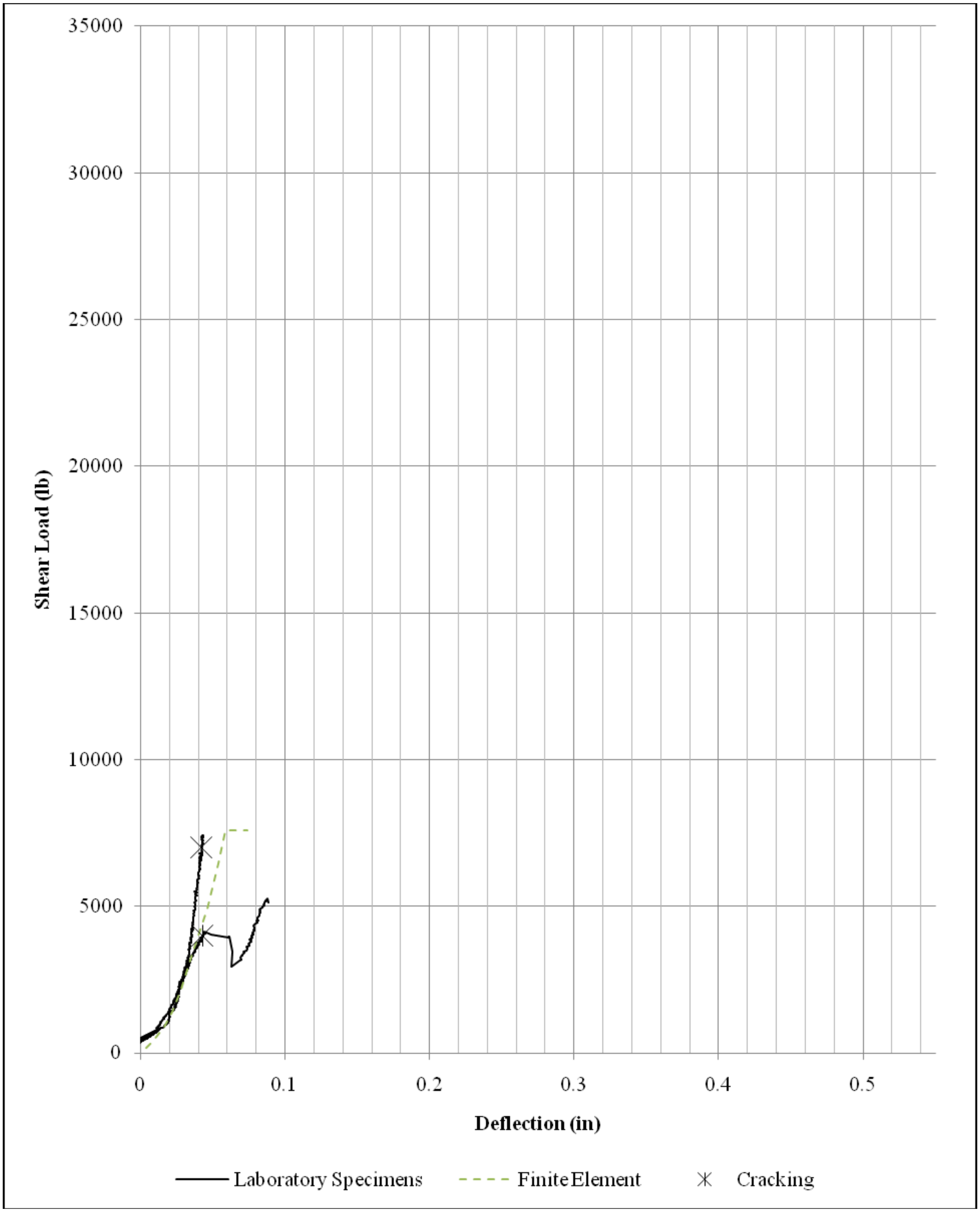

Figure 18. Shear-deflection curves for post-tension type specimens without compression.

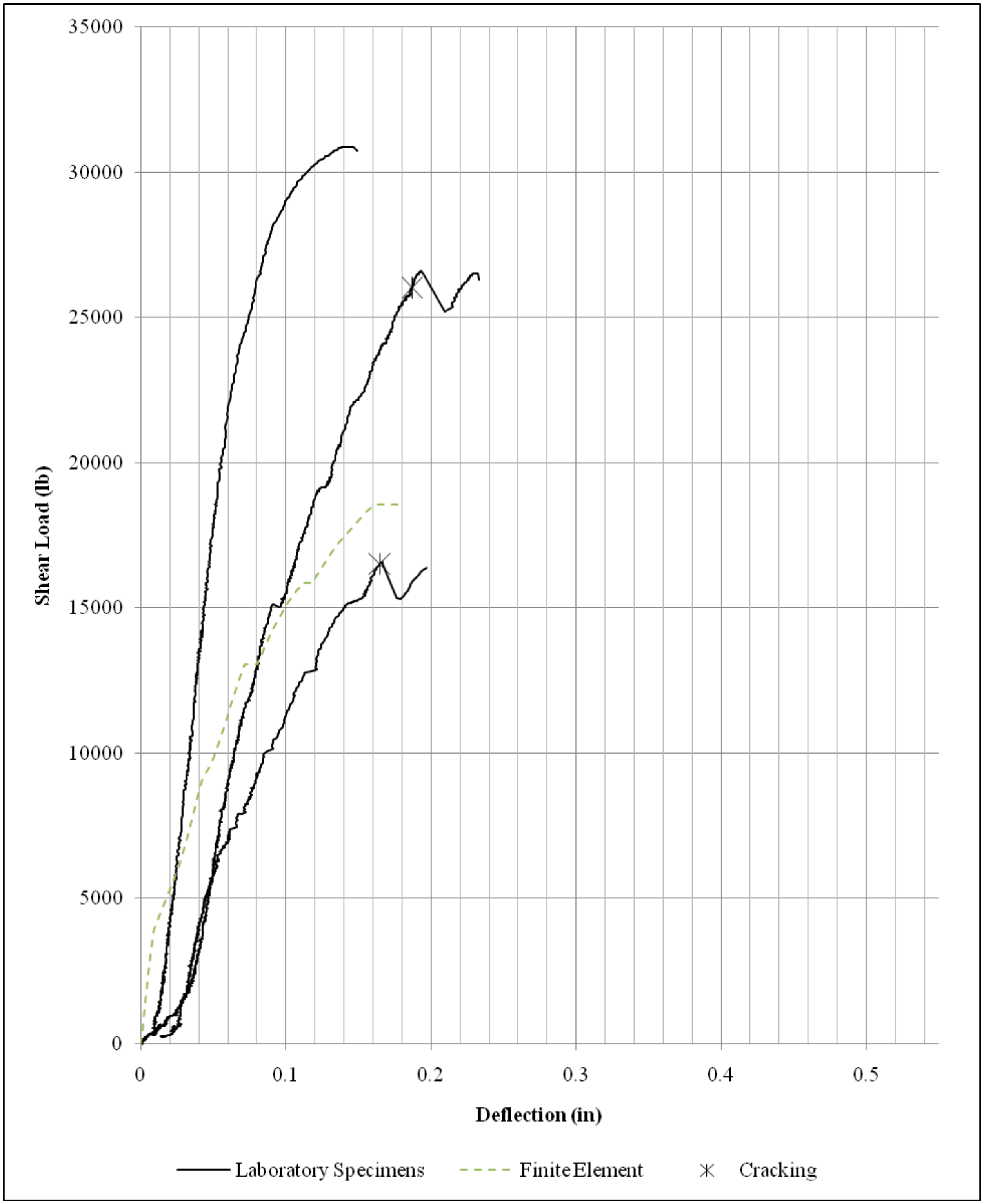

Figure 19. Shear-deflection curves for post-tension type specimens with 300 psi of compression.

Figure 20 shows the ultimate shear capacities for all connections versus concrete compressive strength. The shear capacities of the various connections are shown on the vertical axis with their concrete panel compressive strengths on the horizontal axis. From this figure it can be seen that increased panel concrete strength did not necessarily increase the connection shear capacity. This may be due to the effects of grout strength or simply small sample sizes.

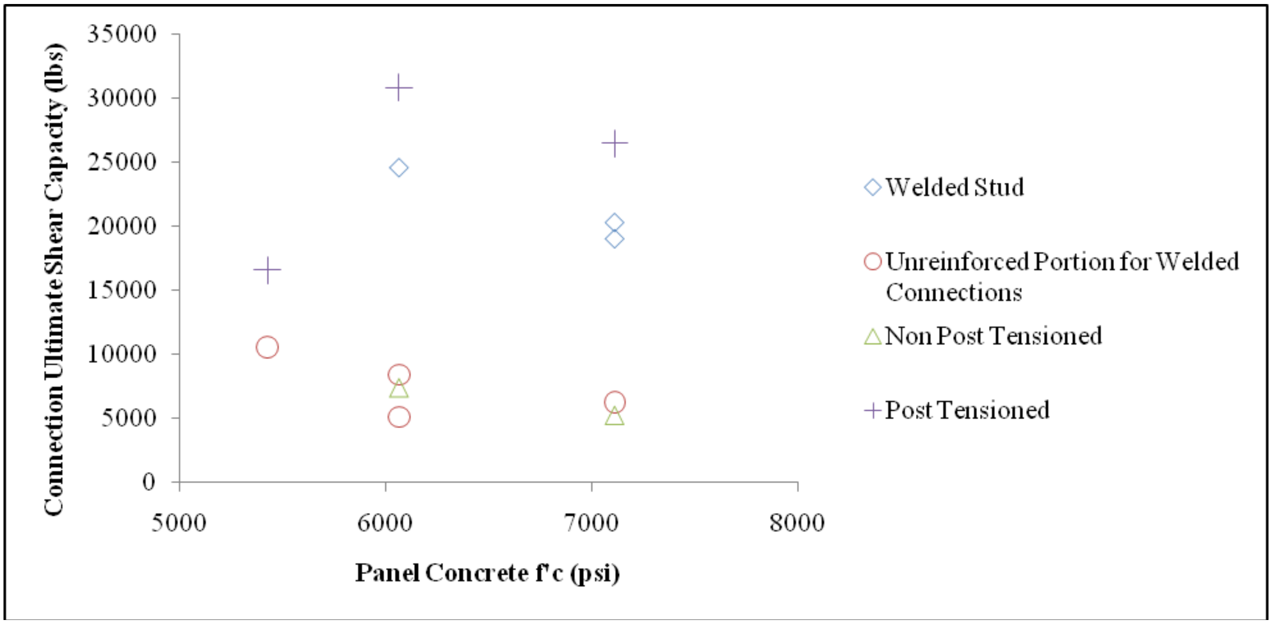

Figure 20. Shear specimen monotonic ultimate capacities.

While Table 9 in the Appendix and Figure 20 seem to imply that the welded stud connection is almost as strong as the post tensioned connection, this is only true for the welded portion of the welded stud connection. The space between each six inch long welded portion of the welded connections in actual bridges is an unreinforced grouted pocket. This unreinforced portion is significantly weaker in shear than the post tensioned connection. Figure 21 shows a comparison of the average capacities for each connection taking into account the unreinforced portions of the welded stud connection. In this figure each connection capacity is given per foot. The continuously welded stud connection is a welded stud connection that has no unreinforced portion. This connection is not used in actual bridges. The other two welded stud connections listed represent those currently in use. The one spaced at 18 inches on center represents a connection having six inches of welded stud followed by 12 inches of unreinforced connection. This is the same connection setup used in the flexural specimens. The connection spaced at 24-inches on center has six inches of the welded stud connection followed by 18 inches of unreinforced connection. Figure 21 shows that the welded stud connections in use are weaker than the post tensioned connection and become weaker the further the connections are spaced.

The average shear capacities of each connection are also compared to each other in Table 2. In this table, the ratio of each connection capacity to the capacity of the post tensioned connection is given. From this table it can be clearly seen that post tensioning almost quadrupled the post tensioned connection's shear capacity. It can also be seen that the welded portion of the welded stud connection is almost as strong in shear as the post tensioned connection. When the unreinforced portions of this connection are taken into account, this connection is only 0.44 to 0.49 times as strong as the post tensioned connection.

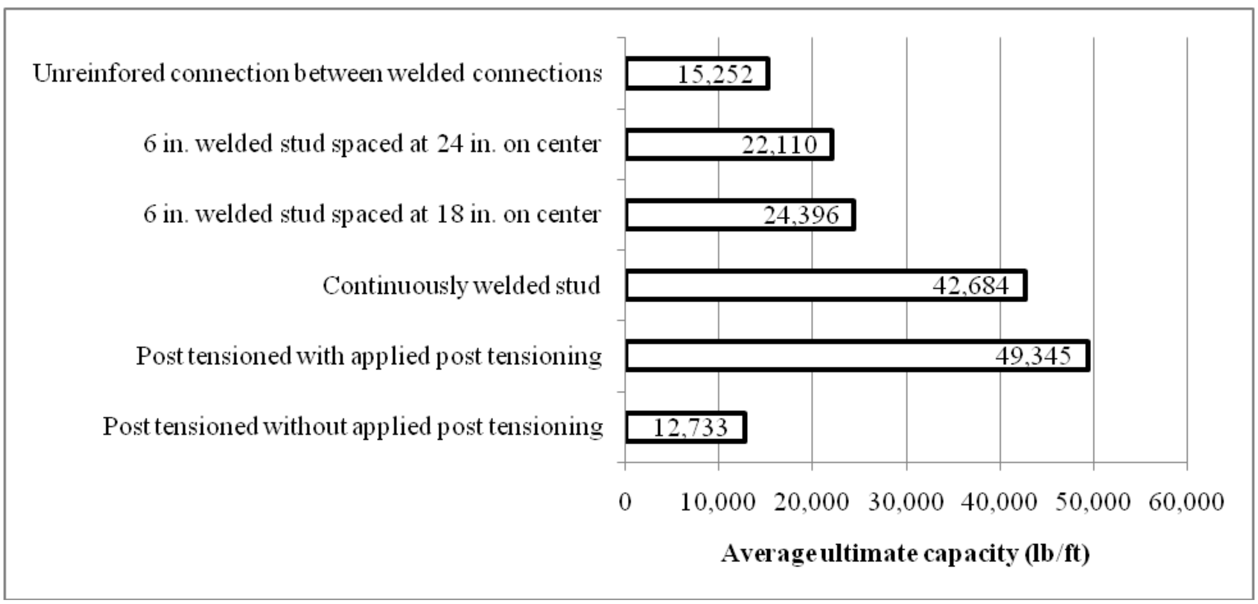

Figure 21. Comparison of average connection shear capacities.

Table 2. Relative Ultimate Shear Strengths of Connections

Connection	Average Ultimate Shear Capacity (lbs/ft)	Ultimate Shear Capacity/Capacity of Post Tensioned Connection
Non-post tensioned	12,733	0.26
Post Tensioned	49,345	1.00
Continuously Welded Stud	42,684	0.87
Welded Stud spaced 18 inches	24,396	0.49
Welded Stud spaced 24-inches	21,706	0.44
Unreinforced Portion for Welded Connections	14,713	0.30

5.1.2 Shear specimen failure modes and cracking

During testing, the cracking of shear specimens was recorded. Table 10 in the Appendix shows the observed cracking at different loads in shear specimens. The cracking loads are approximate and all cracking may not have been noticed. Despite these limitations, Table 10 in the Appendix still shows how each connection fails in shear and allows for a general comparison of cracking loads. Cracking was also marked on Figures 16 through 19 shown earlier. Pictures of all specimens after testing showing cracking are found in Appendix B.

At the end of testing pictures were taken of the final cracking to show how each connection failed. The cracking sequence for a welded stud specimen is shown in Figure 22. In the figure, initial separation occurs between the concrete and grout in the upper left hand side of the pocket. Cracking starts at the location of the welded studs on the left side of the figure as seen in the second picture. This crack continues till the bottom of the connection, and cracking through the bottom of the grouted portion can be seen. Another crack forms along on the opposite side along the welded stud. Towards failure cracking occurred through the grout at an angle of approximately 30° while the studs pulled through the concrete.

Comparatively, ANSYS predicts cracking similar to the tested sequence. Figure 23 shows that cracking began at the point where the welded studs are located. This figure does not show the separation because it is not considered cracking, but it is to be noted that separation between the grout and concrete does occur in the finite model. Figure 23(b) shows the cracking in the grout at approximate a 30° angle. Figure 23(c-e) shows the cracking continuing down the path of the welded stud, and across the grouted pocket. Towards the end of the analysis major cracking occurs on the right side of the model, and upper left portion.

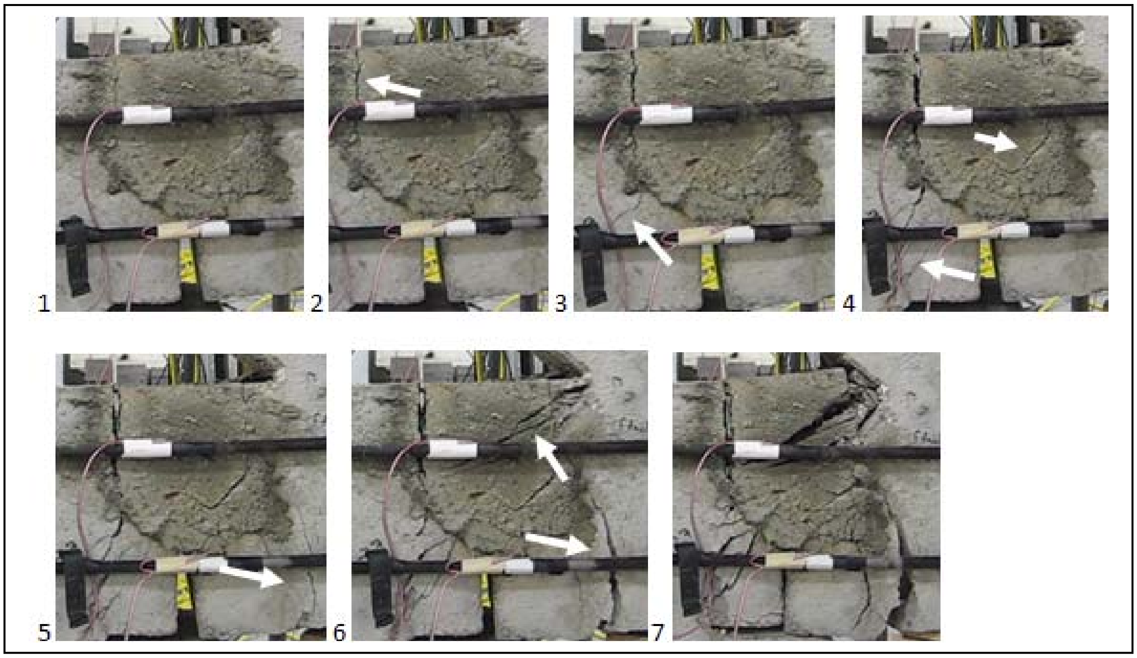

Figure 22. Cracking sequence of a welded stud shear specimen.

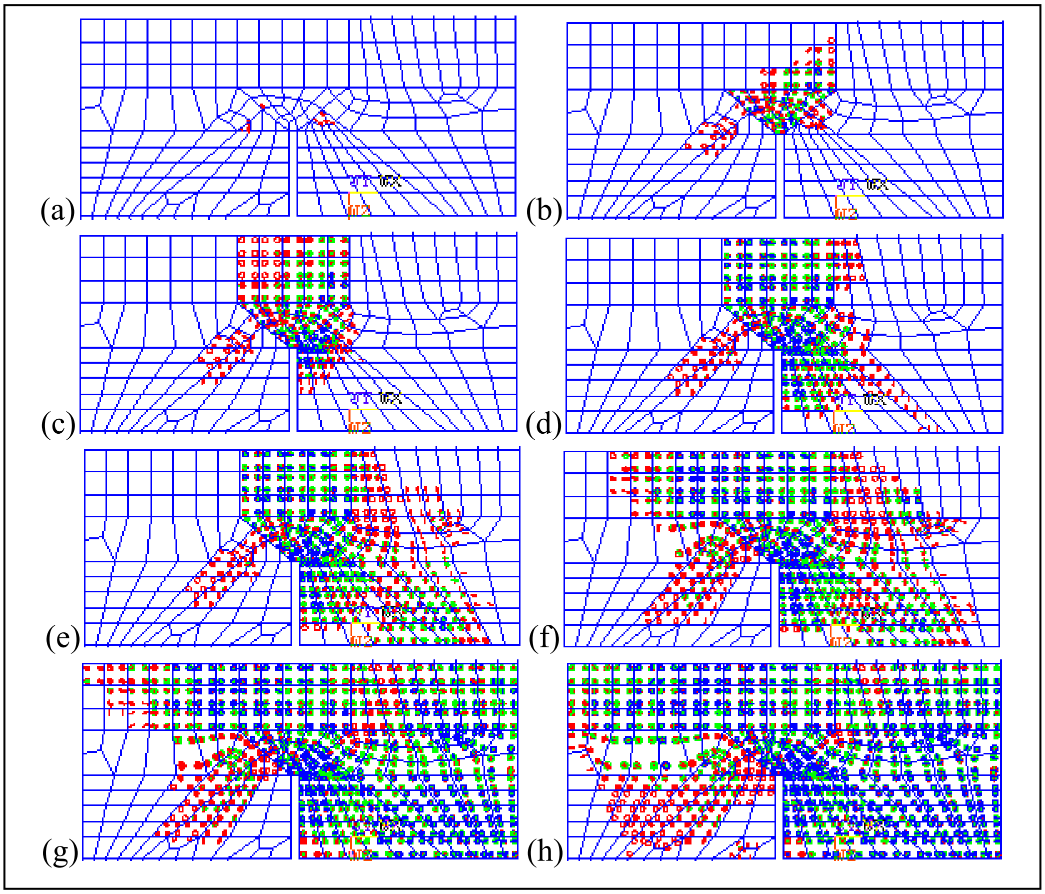

Figure 23. Cracking sequence of welded stud shear finite element model.

Figure 24 shows the cracking sequence for the unreinforced portions for the welded connections. Initial cracking started at the upper right portion of the shear key and continued at approximately a 45° angle. This crack spread into the grout at the same angle and specimens failed along that plane. Failure occurred suddenly and at low loads. Figure 25 shows the cracking sequence that ANSYS predicts. The first initial crack occurs also on the upper right hand side of the shear key. In Figure 25(b-d) cracking spreads from the right corner of the shear key, and downward into the deck area, but multiple cracks primarily occur in the upper right hand portion. In Figure 25(e,f) shows cracking through the grouted portion at approximately a 45° angle.

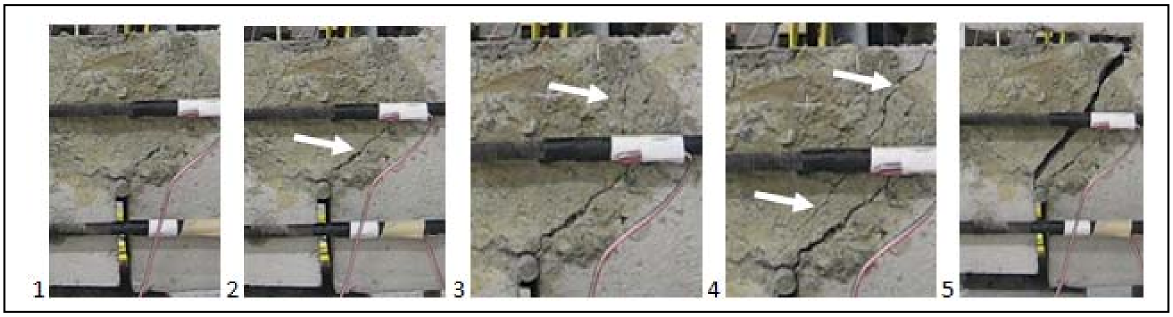

Figure 24. Cracking sequence of an unreinforced shear laboratory specimen for welded connections.

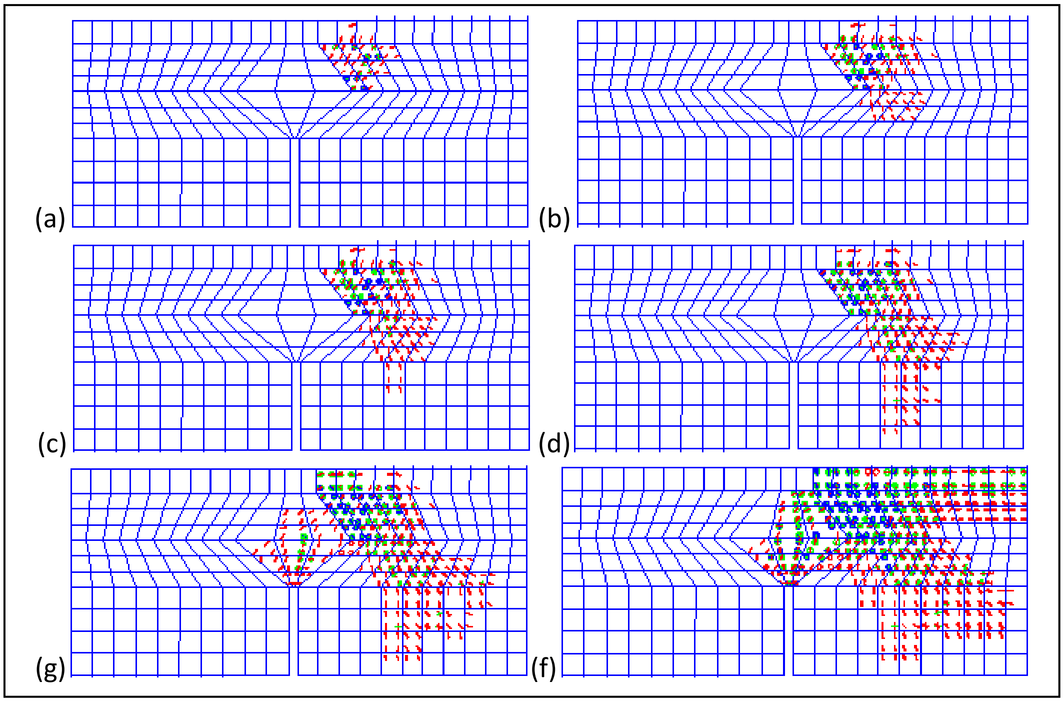

Figure 25. Cracking sequence of the unreinforced shear finite element model for welded connections.

The cracking sequence for a post-tension type connection without compression is shown in Figure 26. Figure 27 shows the finite element predicted cracking sequence. This figure show cracking along the boundary of the grouted pocket, and a cracking at about a 60° angle.

Fig 28 shows the cracking sequence for a post- tension type specimen with 300 psi of applied compression. The post tensioned models fail shortly after cracking occurs. All of the tested models experienced cracking in the flanges. Figure 28 shows the first visible cracks occurring in the flanges, and the cracking in the connection occurring at the bottom left and top right corners of the connection. These cracks continue toward the connection at an angle between 30° and 45°, and continue along the boundary between the concrete and grout.

Similar results were seen in the FE model. Figure 29 shows the cracking in the FE model with 300 psi of compression applied to the connection. The initial cracking in the model was lower than the observed cracking in all tested cases; however, the cracking sequence has a similar pattern in the finite model and the tested results. The predicted cracking also begins in the flanges as is shown in Figure 29 (a). Cracking in the connection begins at the upper right hand side, and lower left hand side, and continue through the grouted pocket (Figure 29 b-d).

Without post tensioning, the connections failed by having a crack form along one side of the grout-concrete interface. Then a diagonal crack spread into the concrete from one of the corners of the connection, causing total connection failure. Adding post tensioning to the connections increased the loads required to crack the connections, but the cracking pattern was about the same. The major differences were that some post tensioned connections had cracks go through the grout, the cracks on the concrete-grout interface tended to be shorter when post tensioned, and the final failure plane was more diagonal when post tensioned.

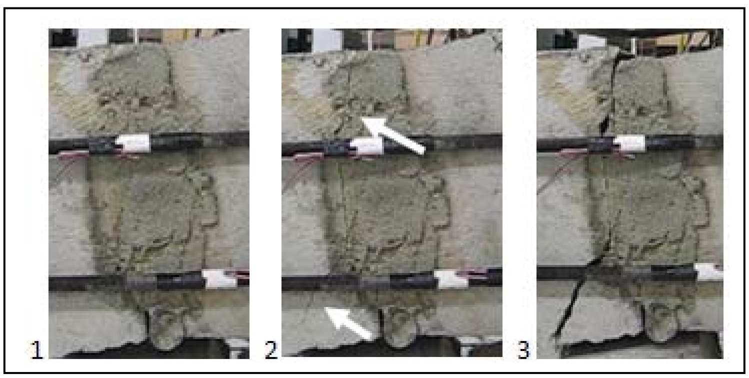

Figure 26. Cracking sequence of a post-tension type shear laboratory specimen without applied compression.

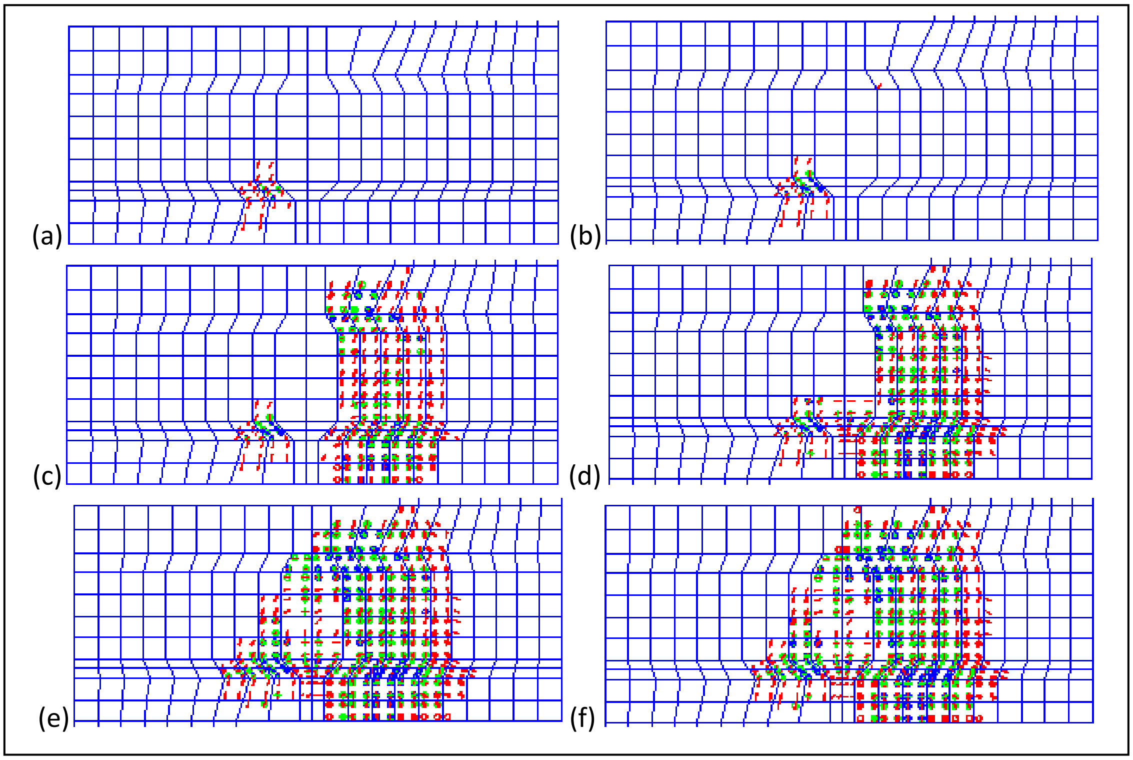

Figure 27. Cracking sequence of the post-tension type finite element shear model without applied compression

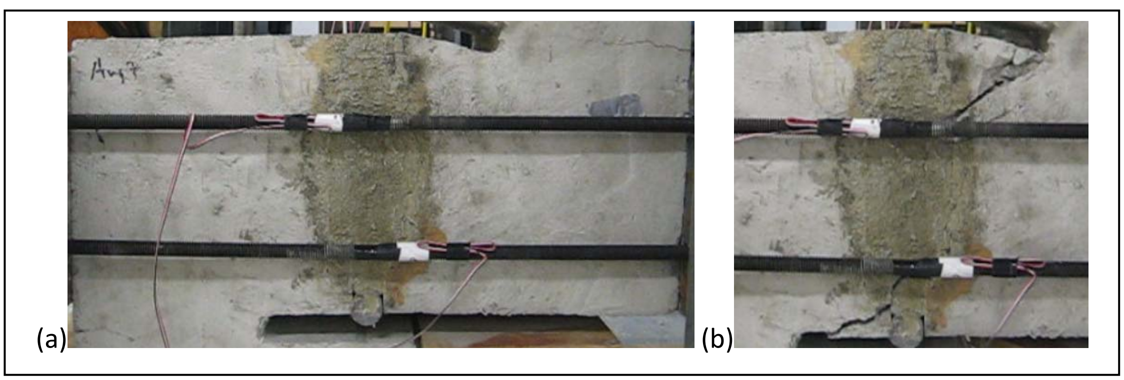

Figure 28. Cracking sequence of a post tension type shear laboratory specimen with applied compression.

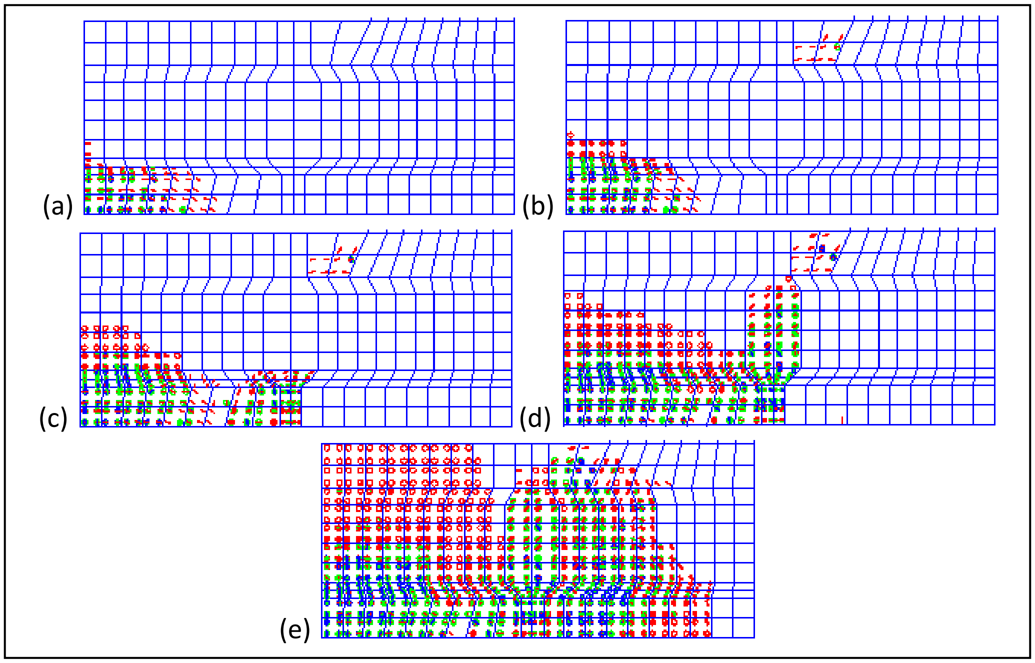

Figure 29. Cracking sequence of the post tension type finite element shear model with applied compression.

5.2 Cyclic Shear Test Results

Shear specimens were also tested in a high-amplitude, low-cycle cyclic load test. Information for each specimen, including concrete cast date, grout date, and testing date can be found in Table 12 in the Appendix. First, at least three shear specimens of each connection type were tested monotonically to failure. Cyclic specimens were then tested by loading them to 90% of the mean minus one standard deviation of their ultimate failure load. This was chosen because it provided a low enough load that no specimens should have failed during the first load cycle. At the same time it was a high enough load that it should have produced failure in a reasonable number of cycles. If specimens did not fail after 30 cycles of loading, then the load was increased by 500 lbs for 3 cycles, and then increased by 500 lbs for another 3 cycles and so on until failure occurred. Results of these tests are shown in Table 3. This table shows the cycle number when failure occurred and the maximum load for that cycle.

During cyclic testing, many of the samples failed away from the connection showing that the test setups were prone to cyclic failure and not necessarily the connections. In most other cases the connections failed at about the same loads as in the monotonic tests. For these reasons, the cyclic shear tests are either inconclusive due to lack of data or they show that these connections are not prone to high amplitude, low cycle fatigue.

Two tests where the post tensioned specimens failed away from the connection do show that the connections had the ability to withstand high amplitude fatigue. The first post tensioned specimen failed away from the connection after the connection had withstood 20,000 lbs of shear. This load was higher than the failure load for one of the monotonic shear specimens implying that the cyclic nature of the load had no effect on shear capacity. The third post tensioned specimen also failed away from the connection at a load higher than one of the monotonic shear specimens. Both specimens failed after over fifty cycles of loading.

Only one cyclic test was run on the non-post tensioned connection, but this test implied that this connection may be prone to high amplitude fatigue. The specimen failed in the connection during the twenty fifth cycle of loading. This should not be a concern in actual bridges as this connection is post tensioned in practice.

The welded stud connection and the unreinforced portion for the welded connections both failed at loads similar to the monotonic tests. Table 4 shows a comparison between the average monotonic shear capacities and the average cyclic capacities. This table shows that the cyclic and monotonic failure loads are similar. The unreinforced portion for welded connections and the non-post tensioned connections failed at 75% and 71% (respectively) of their connection's average monotonic capacities; however, these averages were based on 1 or 2 specimens and the failure loads on the unreinforced connection were within the range of the monotonic specimens so this may not mean they are weaker in cyclic loading.

Table 3. Shear Specimen Cyclic Capacities

Connection	Specimen #	Panel f'c (psi)	Cycle at Failure	Cycle Load (lbs)
Welded Stud	1	6066	52	20000
	2	5427	13*	16500
Unreinforced Portion for Welded Connections	1	7113	37	6000
	2	6066	32	5000
Non-Post Tensioned	1	5427	25	4500
Post Tensioned	1	6066	55**	20000
	2	5427	8**	15500
	3	5427	52**	19000
	4	7113	96	26500

*Failure caused by specimen twisting. This is considered to be a problem with the specimen and not a cyclic failure.

** Failed away from connection. This is a problem with the specimen and not cyclic failure in the connection.

Table 4. Shear Specimen Average Cyclic vs. Monotonic Capacities

Connection	Average Monotonic Capacity (lbs)	Average Cyclic Capacity (lbs)	Ratio of Cyclic/Monotonic
WS	21342	20000	0.94
UR	7357	5500	0.75
NPT	6367	4500	0.71
PT	23983	26500	1.10

WS=welded stud, UR=unreinforced portion for welded connections, NPT=non-post tensioned, PT=post tensioned

While the results of cyclic testing somewhat imply that these connections are not prone to high amplitude, low cycle fatigue, this does not mean that they are not affected by fatigue. The connections also need to be tested in low amplitude, high cycle fatigue to determine if that would be an issue. Also, because of the low sample size in this research, and the few samples that failed in the connection, more high amplitude, low cycle tests could be performed to prove that the connections are not prone to this type of fatigue. In future tests it is recommended that the arm of the specimen (part away from the connection) be made wider and reinforced more.

5.3 Flexural Test Results

5.3.1 Flexural specimen ultimate capacities

Each flexural specimen was loaded until failure to obtain the connection ultimate capacity. Information for each specimen, including concrete casting, grouting, and testing dates can be found in Table 12 in the Appendix.

The moment-deflection curves for each connection type are shown in figures 30 through 32. In these figures the deflections in inches are shown on the horizontal axis while the moments in lb-ft are shown on the vertical axis. Observed cracking is also shown in the figures using markers. The panels usually deflected linearly until cracking occurred, then deflected nonlinearly as the stiffness was reduced up through failure. The rate of deflection varied depending on connection type.

Fig. 30 shows the moment-deflection curves for the welded stud and welded rebar specimens. This figure shows that both welded style connections deflected more rapidly than the other connections. Both connections deflected nonlinearly after cracking. The welded rebar connection’s deflections remained linear much longer than the welded stud connection and was a stronger connection overall.

The welded stud connection is the weakest connection tested in flexure with capacities ranging from 4,400 to 8,500 lb-ft. This was expected because a six inch stud does not provide much anchorage for the connection. The finite element moment deflection curve closely followed the moment-deflection curve for the strongest welded stud specimen. The FE predicted cracking moment was at 1,764 lb-ft, which is relatively low compared to the observed cracking moment recorded from the tested specimens. However, there is a second point of cracking where major deflection occurs, and this point is considerably closer to the observed cracking moment. This happens at 3,284 lb-ft and is recognized as the first plateau seen on the moment-deflection graph.

The welded rebar connections were much stronger than the welded stud connections with capacities close to the post tensioned connections. This is probably because the long section of rebar extending into the deck is much better anchored than Nelson studs are. This makes the connection region similar to the rest of the panel. Initial FE modeling of the welded rebar modeled without contact elements produced a similar moment-deflection curve as the laboratory results. This is due to a small linear region before cracking, where the finite element models proved to be much stiffer without the contact pairs. Surprisingly the initial cracking calculated in ANSYS occurs around 2,500 lb, while the recorded cracking during the laboratory testing occurs between 7,200 lb-ft to 13,700 lb-ft. A second point of major cracking with an increased deflection occurs at 11,059 lb-ft, which is within the range of the observed cracking. This second point of cracking is the small plateau seen in the ANSYS moment-deflection curve.

Fig. 31 shows the moment-deflection curves for the post tensioned specimens. This figure shows that the post tensioned specimens had the least deflection for a given load and remained linear for relatively high loads as expected. Post tensioning keeps the connection in compression for higher loads preventing cracking and grout separation. The finite element moment-deflection curve follows the tested curves almost exactly in the linear range prior to cracking. After cracking the finite element model follows the highest strength specimen. The cracking moment for the finite element model is 13,982 lb-ft.

The moment-deflection curves for the 24-inch and 36-inch curved bolt specimens are shown in Figure 32. This figure shows that the longer curved bolt specimens performed better than the shorter curved bolt specimens. The longer specimens deflected slowly until reaching about 5,000 N-m of moment and then started deflecting at about the same rate as the welded rebar connection. The shorter curved bolt specimens cracked and went nonlinear before reaching 5000 N-m of moment, deflected rapidly, and then started taking additional load. The 36-inch specimens were slightly stronger than the post tensioned specimens.

Initial FE analysis of the curved bolt connections resulted in moment-deflection curves that were extremely rigid until the point of cracking. After cracking the models deflected without additional load, and then followed the trend of the laboratory moment-deflection curves until termination of the analysis. In an attempt to improve the results contact pairs were added along the concrete grout interface. The models with the added contact pairs had a similar curve to the tested specimens, but at the point of cracking the model deflected without added load, and resulted in a softer curve than the tested results. Finally, to obtain accurate results it was assumed that the tested beams had cracking previous to testing. In order to model the beam being cracked, the model was loaded until the cracking moment, unloaded, and loaded to the full amount. The curve of the initially cracked curved-bolt finite element models closely follow the tested results. The 24-inch curved bolt FE moment-deflection curve follows the tested specimens but lacks their initial rigidity. The tested specimens initially have a rigid linear region, then around 3,000 to 4,000 lb-ft the deflection increases, and a more gradual curve follows. The modeled analysis does not show this trend but otherwise closely follows the laboratory results.

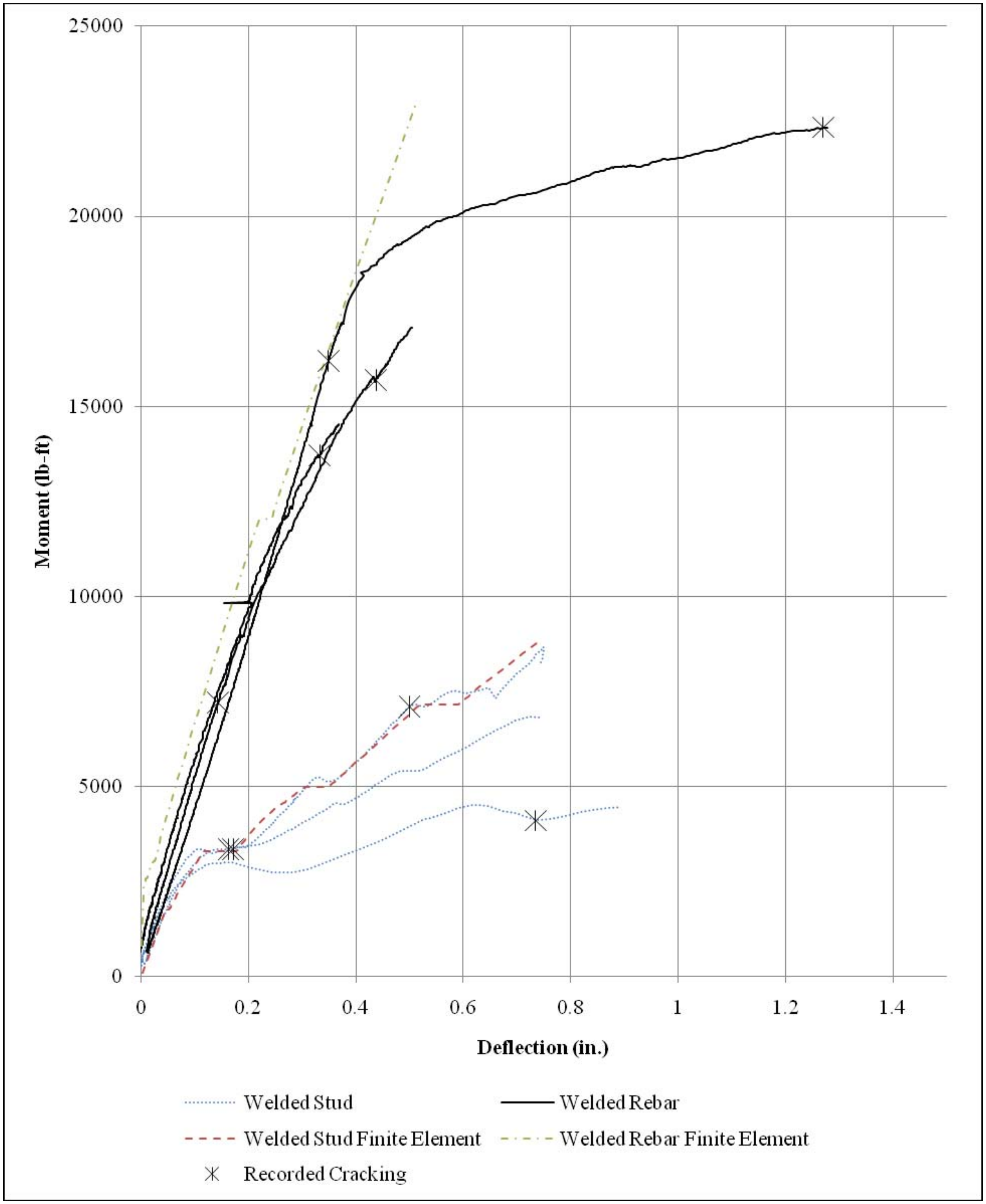

Figure 30. Moment-deflection curves for welded stud and welded rebar specimens.

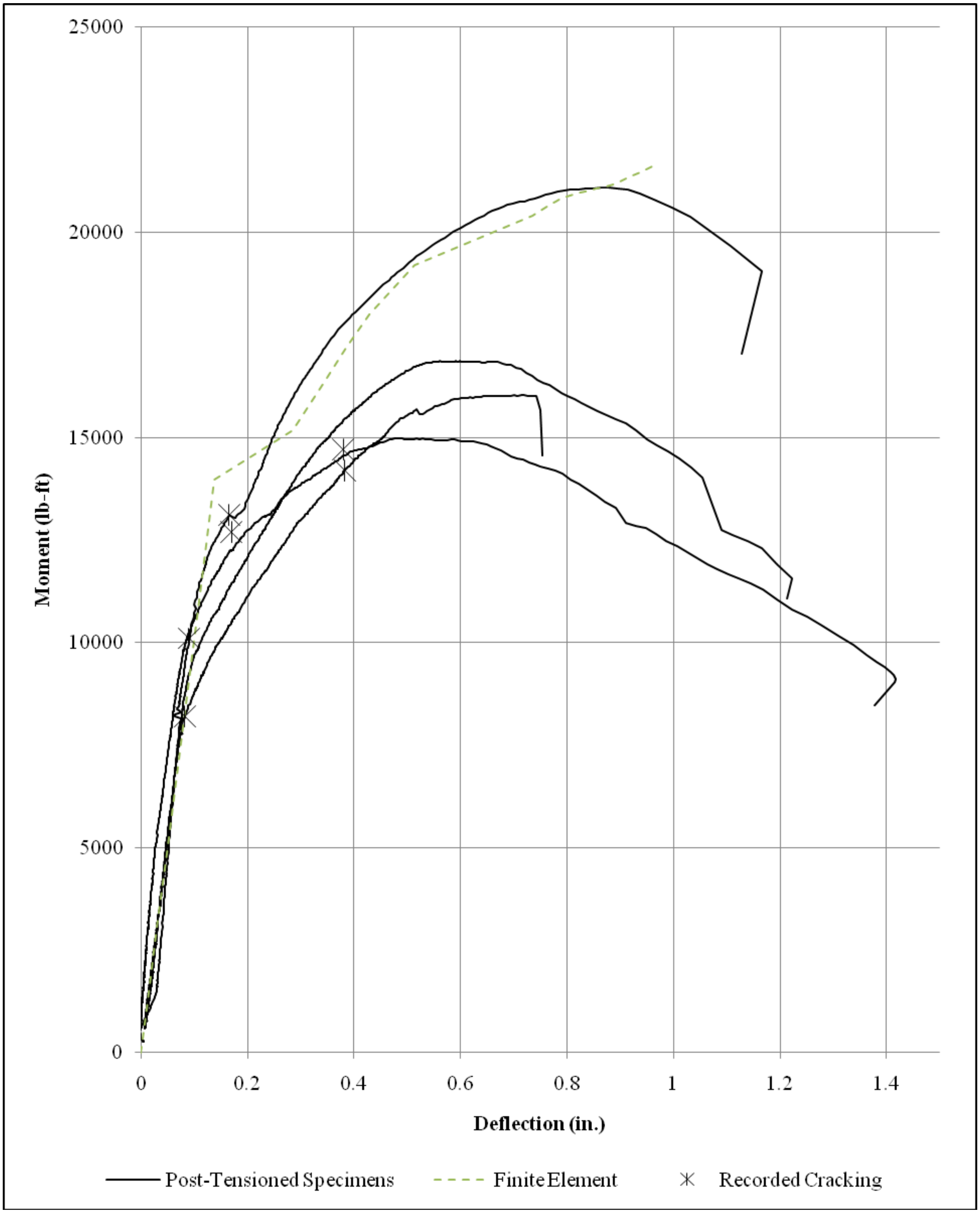

Figure 31. Moment-deflection curves for post tensioned specimens.

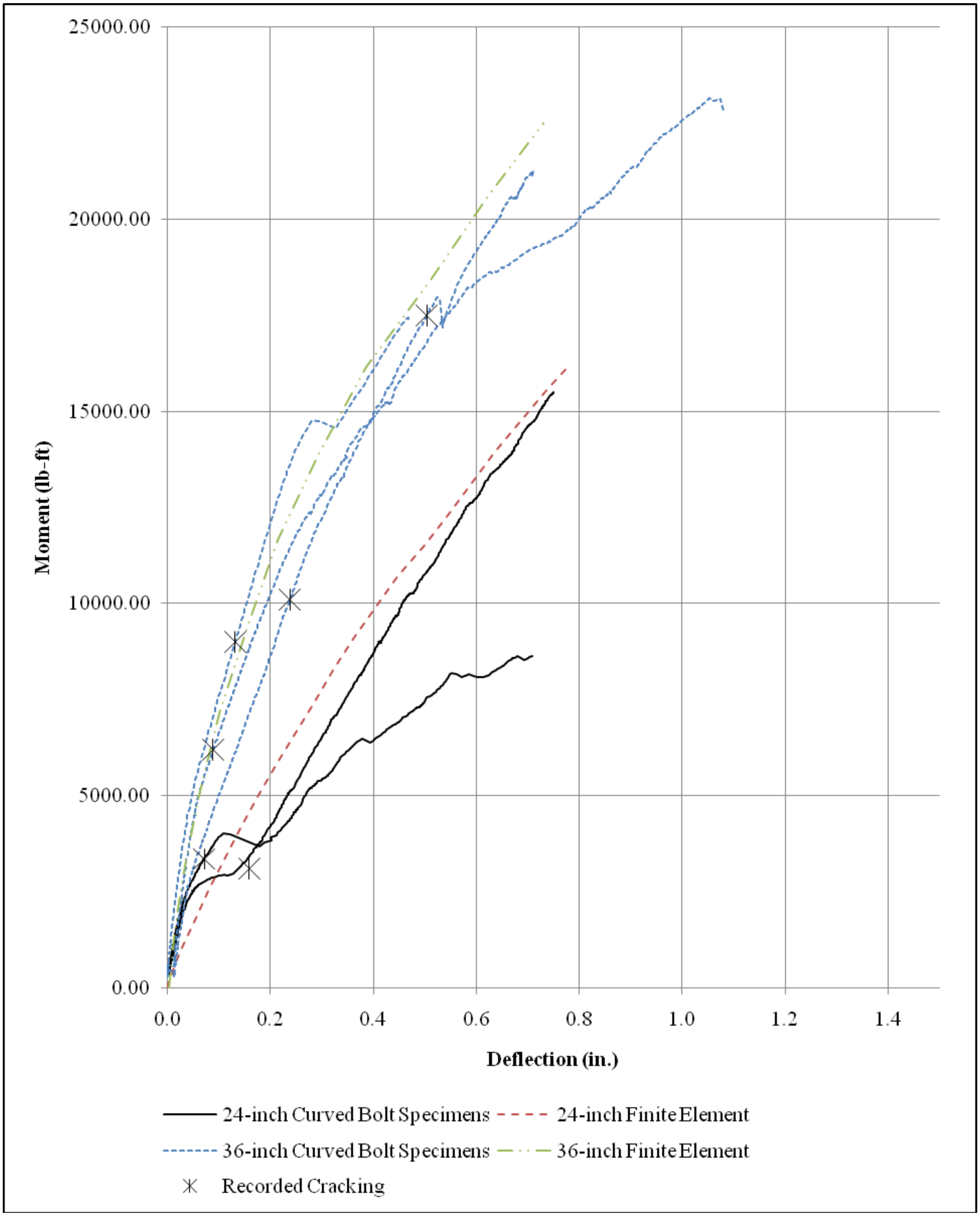

Figure 32. Moment-deflection curves for 24 and 36 inch long curved bolt specimens.

Table 7 in the appendix shows a summary of the flexural specimen ultimate capacities. These capacities are shown graphically in Figure 33 with capacity on the vertical axis and concrete compressive strength on the horizontal axis.

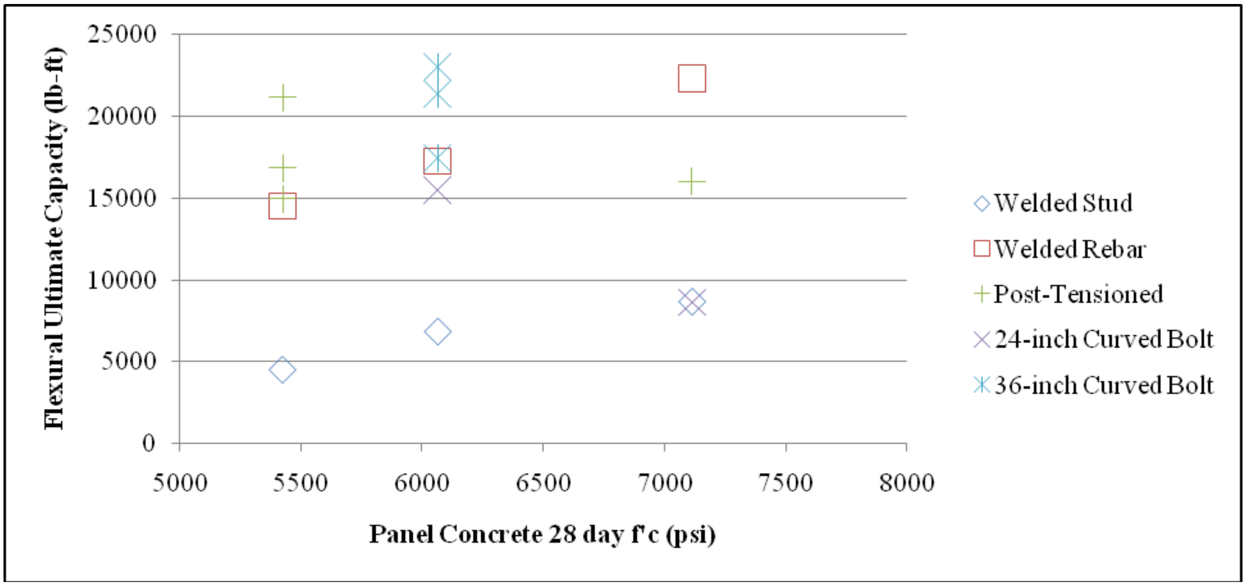

Figure 33. Flexural specimen ultimate capacities versus concrete 28 day compressive strength.

The average flexural test specimen capacities can also be compared to each other. Figure 34 shows the average capacity of each connection type graphically. Connections were cast on different dates and consequently have different concrete strengths. For example, the 36-inch curved bolt connections were all cast on September 18, 2008 so they have that day's concrete strength whereas the welded connections had one specimen cast on each casting date. Because of this, comparisons between averages are not meant to be exact, but rather show connection trends.

Table 5 shows a comparison of the average flexural capacities for each connection type. In this table, all the connections were compared to the post tensioned connection because it is UDOT's preferred connection and a connection with known good field behavior (Issa 1995b). This table shows that the welded rebar connection is significantly stronger than the welded stud connection. It was 2.7 times as strong as the welded stud connection. The welded rebar connection is even slightly stronger than the post tensioned connections. The 24-inch curved bolt connection is about 0.70 times as strong as the post tensioned connection and significantly stronger than the welded stud connection. Meanwhile, the 36-inch curved bolt connection was the strongest connection tested. This implies that the curved bolt connection can be used to effectively post tension a connection. It also shows that the longer the curved bolt connections are better at post tensioning a connection. The moments associated with the first seen cracking are also given and compared to the first cracking of the post tensioned connection. Finite element model predicted capacities and cracking moments are also given and ratios of specimen capacity to finite element model capacity and specimen cracking moment to finite element cracking moment are given. The theoretical flexural capacity of continuous panels is also given for concrete compressive strengths from 4 ksi to 7.11 ksi, including the strengths of all panel concrete tested in this research. Ratios of connection laboratory tested capacity to theoretical continuous panel capacity are given in the table.

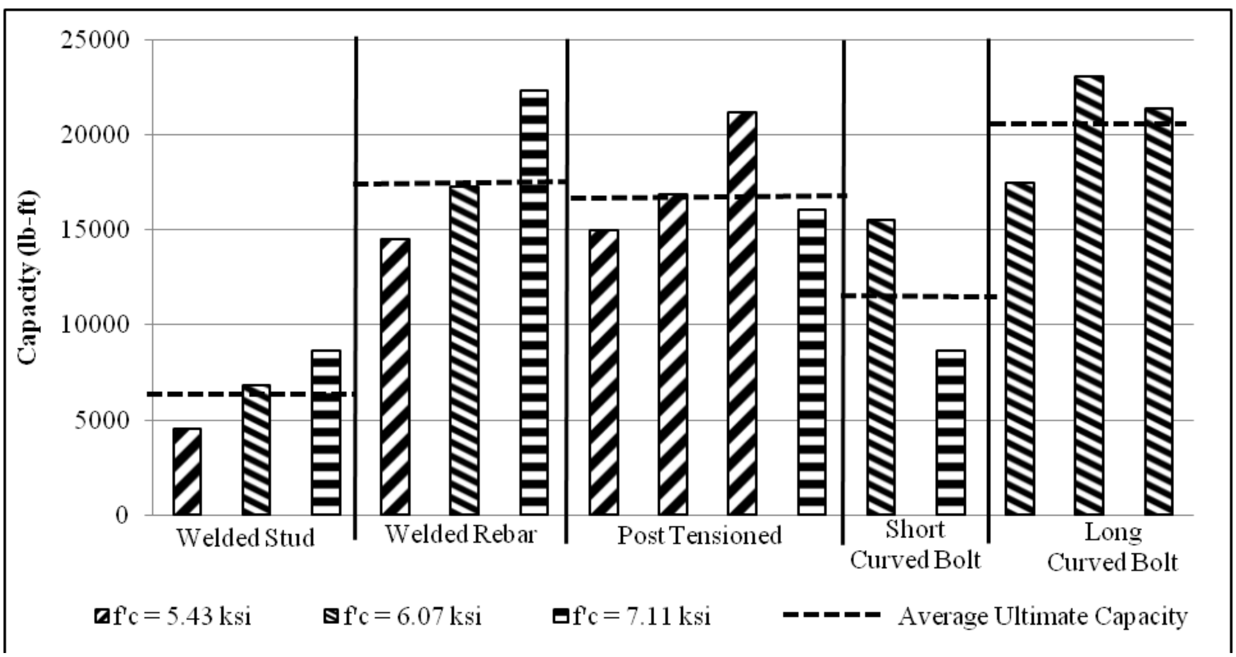

Figure 34. Flexural specimen ultimate and average capacities.

Table 5. Relative Average Flexural Specimen Capacities

Connection	Moment at First Seen Cracking lb-ft	First Crack/ PT First Crack	Ultimate Flexural Capacity lb-ft	FE Ultimate Capacity lb-ft	Capacity/ Continuous Capacity	FE Capacity / Capacity
Welded Stud	3,350	0.41	6,667	8,800	0.16	1.31
Welded Rebar	7,200	0.88	18,047	22,920	0.44	1.27
Post Tensioned	8,200	1.00	17,261	21,640	0.42	1.25
Short Curved Bolt	3,100	0.38	12,079	16,250	0.29	1.34
Long Curved Bolt	6,200	0.76	20,623	22,500	0.50	1.09
Continuous, f'c=4 ksi	-	-	37,968	-	1.00	-
Continuous, f'c=5.43 ksi	-	-	40,604	-	1.00	-
Continuous, f'c=6.07 ksi	-	-	41,194	-	1.00	-
Continuous, f'c=7.11 ksi	-	-	41,931	-	1.00	-

5.3.2 Flexural specimen failure modes and cracking

During the flexural tests the cracking of test panels was recorded along with the corresponding cracking loads. Table 12 in the Appendix shows a summary of observed cracking during flexural testing. This table is approximate and while it provides a good summary of observed cracking, it may be missing cracking not noticed by the researchers. In some cases the sound of cracking was noticed before any visible cracks appeared. Separation of the grout from the concrete was also observed in many tests. Photographs of all connections after testing are included in Appendix B.

Figure 35 shows the sequence of cracking for a welded stud connection. This connection started cracking with the grout separating from the concrete. Then cracks started forming in the panel concrete. These were noticed on the underside of the panels running parallel to the connection at the location of the ends of the welded studs. Cracks also spread from the corners of the diamond shaped grouted pockets. Finally, the welded studs pulled completely out from the panels and the entire specimen fell.

The cracking sequence for the FE modeled specimens can be seen in Figure 36. Cracking in the computer model starts in the elements surrounding the welded stud. In Figure 36 (b-d) the cracking continues along the area of the welded stud, and the elements beneath, and starts cracking in the grouted pocket. Toward the end of the analysis the majority of the multiple cracks that occur are around the welded plate and along the shear stud.

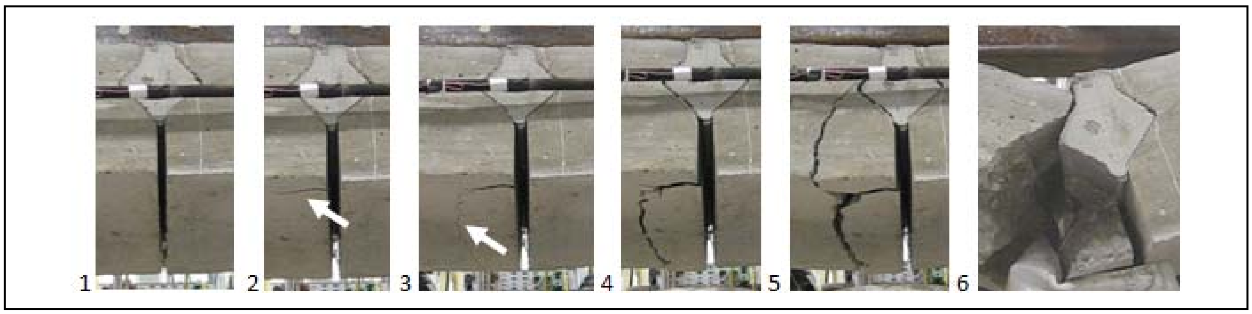

Figure 35. Cracking sequence of a welded stud flexural laboratory specimen.

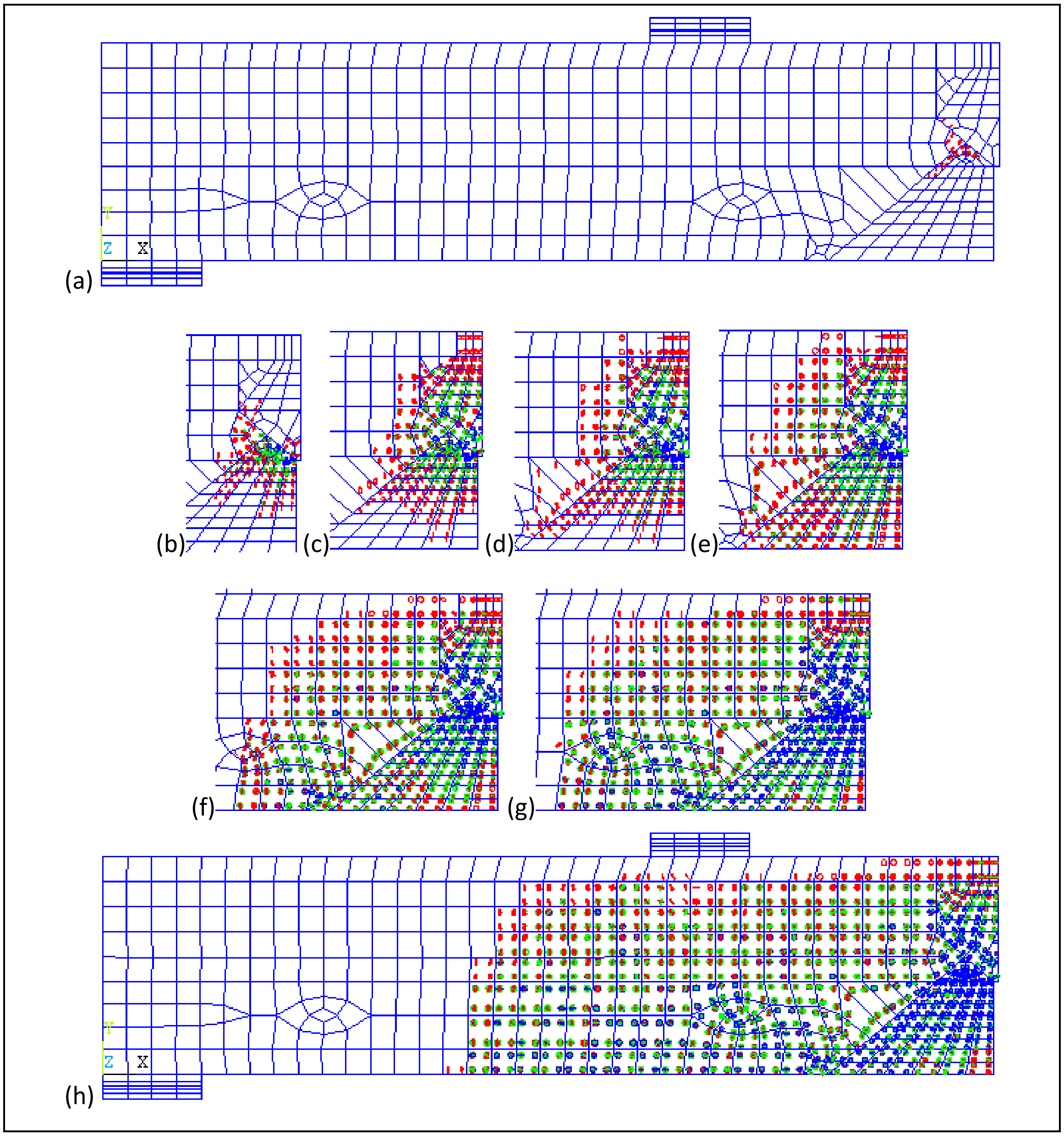

Figure 36. Cracking sequence of the welded stud flexural finite element model.

The welded rebar specimens proved to be much more resistant to cracking that the welded stud connections. Table 12 in the Appendix shows that cracking for this connection was noticed at higher loads than for the stud connections. Figure 37 shows the cracking sequence for this connection. Cracking began in the concrete at the bottom of the grouted pocket where connection plates are welded. Figure 37(b,c) shows the crack continue along the angle of the plate and into the concrete. Ultimate failure occurs at an angle that extends from the plate to the loading point. This cracking sequence is compared with the predicted cracking obtained from the finite element model shown in Figure 38. The cracking begins in the model near the corner of the welded plate between the concrete and grout. In Figure 38(b) multiple cracks occur along the angle of the plate, and the reinforcement. Multiple cracks follow the welded rebar further into the concrete, and multiple cracks occur in the concrete in Figure 38(c-e).

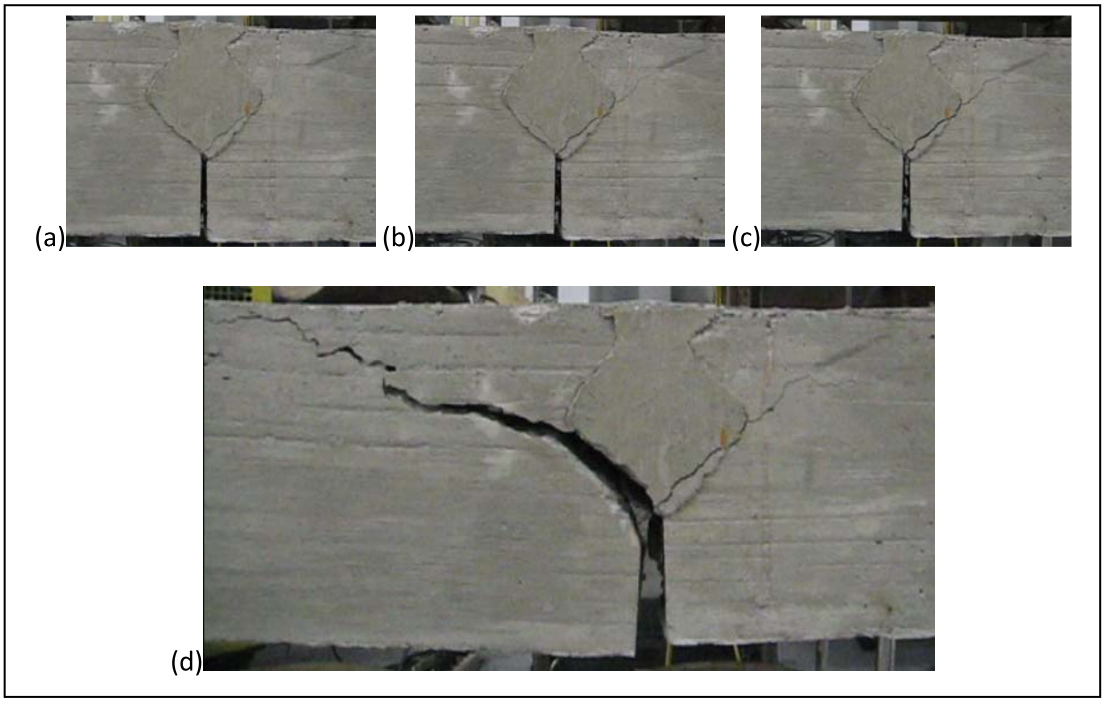

Figure 37. Cracking sequence of a welded rebar flexural laboratory specimen.

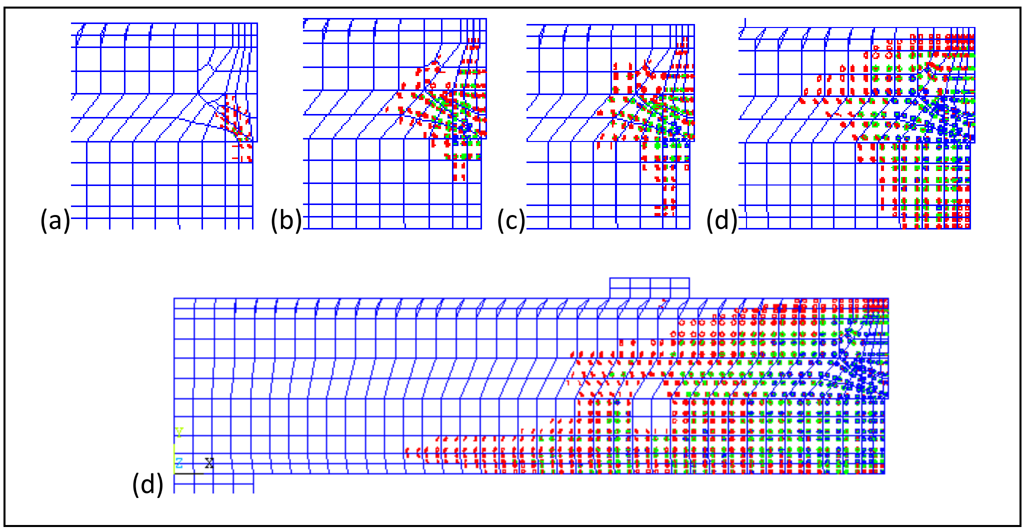

Figure 38. Cracking sequence of the welded rebar flexural finite element model.

Post tensioned connections cracked at high loads. The sequence of cracking for this connection is shown in Figure 39. The cracks began with a small horizontal crack through the top of the grouted pocket. The crack formed where the pocket narrowed. Then the grout and concrete below this crack began to separate while cracks extended from the top corner of the grouted pocket into the panel concrete. At failure there was localized crushing of the deck concrete near the grouted pocket.

Figure 40 shows the cracking sequence calculated by ANSYS. The cracking sequence as predicted in ANSYS shows the cracking initiating in the concrete at the bottom portion of the connection as shown in Figure 40(a). This cracking continues upward and along the connection. Cracking in the grout occurs in the last two steps in the figure, and begins in the bottom of the grouted pocket and moves upwards.

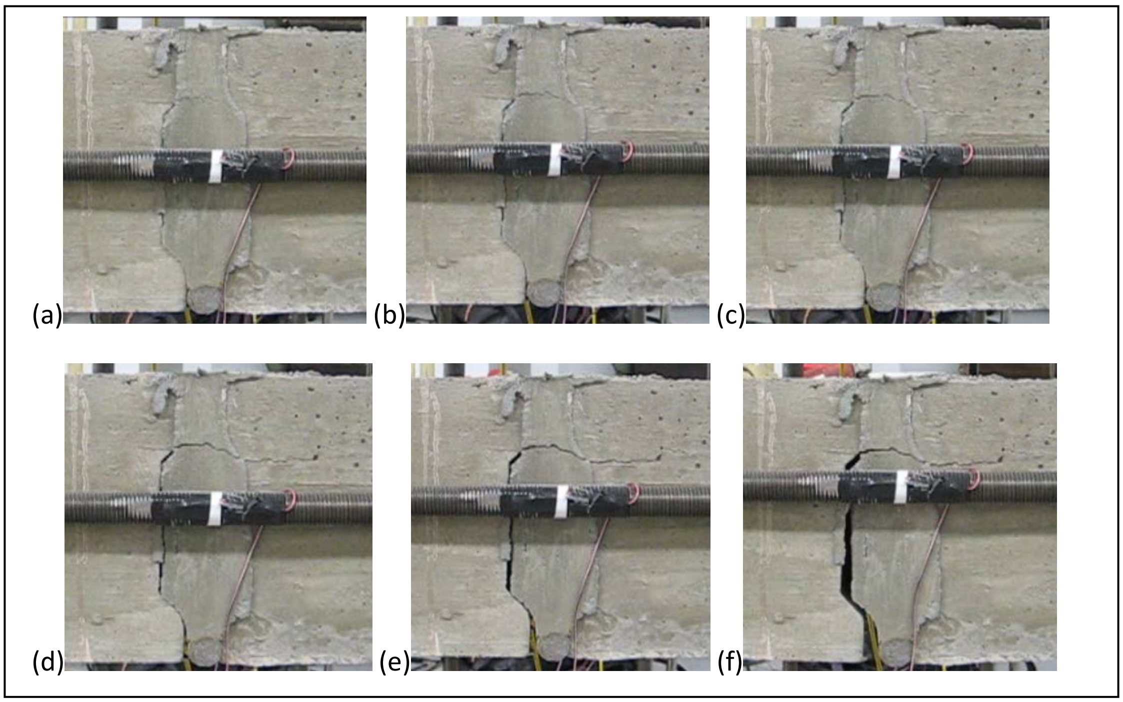

Figure 39. Cracking sequence of a post tensioned tested flexural laboratory specimen.

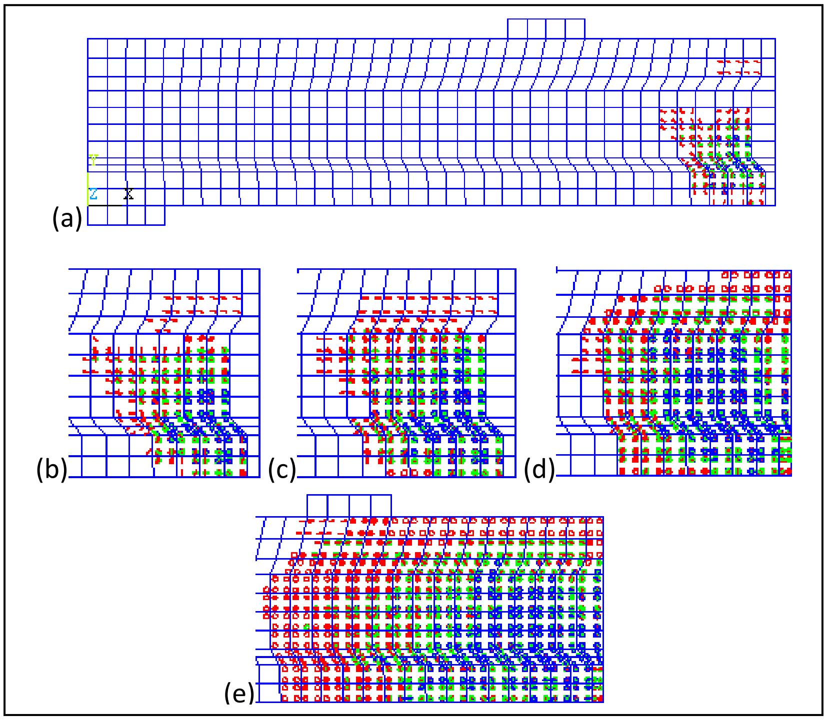

Figure 40. Cracking sequence of the post tensioned flexural finite element model.

The curved bolt specimens failed in similar ways, regardless of bolt curvature. In Figures 41 and 42 the cracking sequence for 24-inch and 36-inch curved bolt specimens, respectively, are shown. Cracking across the grout was noticed similar to that seen in the post tensioned connections. These cracks occurred where the grouted pocket narrowed at the top. Then cracks were noticed spreading from a top corner of the grouted pocked moving towards the end of the curved bolt. These cracks roughly followed the location of the curved bolt conduits. In the 24-inch long connection, the cracks met the top of the deck panels at roughly the same location as the ends of the bolts at failure. Localized crushing of the concrete occurred there. The 36-inch long connection was tested with the loading points closer to the connection to obtain the required failure moment. Perhaps because of this, the cracks in this connection followed the bolt conduits until they came to the loading points and then went nearly vertical. When the cracks met the surface of the deck panel, localized crushing of the concrete occurred. While all of this cracking was happening, separation of the grout from concrete was observed in the lower portion of the panels.

Cracking was seen in the 24-inch long curved bolt connection around 3,000 lb-ft, which was about the same load as the welded stud connection panel cracking (grout separated from concrete at lower loads in the welded stud specimens). These two connections had the lowest cracking loads – less than half those of the welded rebar and post tensioned connections. The 36-inch long curved bolt connection cracked at about 6,000 lb-ft, or about twice the cracking load for the welded stud or shorter curved bolt connections. This was also about three fourths of the cracking load for the post tensioned connection and close to the welded rebar cracking load. This shows that the curved bolt connection has cracking problems if too short. As long as the bolt is long enough it will crack at similar loads to the post tensioned connection.

Figure 43 shows the cracking sequence for the 24 inch curved bolt connection FE model. The first cracks in ANSYS happen while the post tensioning is applied. These cracks occur around the curved bolt area, and when the full 300 psi is achieved across the connection the entire region above the curved bolt is shown as having initial cracking. The model cracks similarly to the 36 inch curved bolt model.

Figure 44 shows the FE cracking sequence for the 36 inch curved bolt model. The cracking pattern is somewhat different than that observed in the laboratory specimens and could be accounted for by the way the curved bolt was modeled. In the tested specimen there was an oversized conduit, and when the tensile force was applied to the bolt it interacted with the conduit creating a vertical force as aforementioned. This may not be accurately represented in the ANSYS model because the curved bolt had direct contact with the concrete, and the tensile force was provided due to thermal expansion. Cracking does occur in the model above the curved bolt at the final cracking stages, but initial cracking starts at the bottom of the beam below the left end of the curved bolt. Figure 44(a) shows the initial cracking around the curved bolt after the post tensioning is applied. The next cracking occurs at the mentioned location below the curved bolt. This spreads upwards through the thickness of the modeled deck. Cracking occurs at this location because after the curved bolt area is put into compression, this point has the highest tensile stresses.

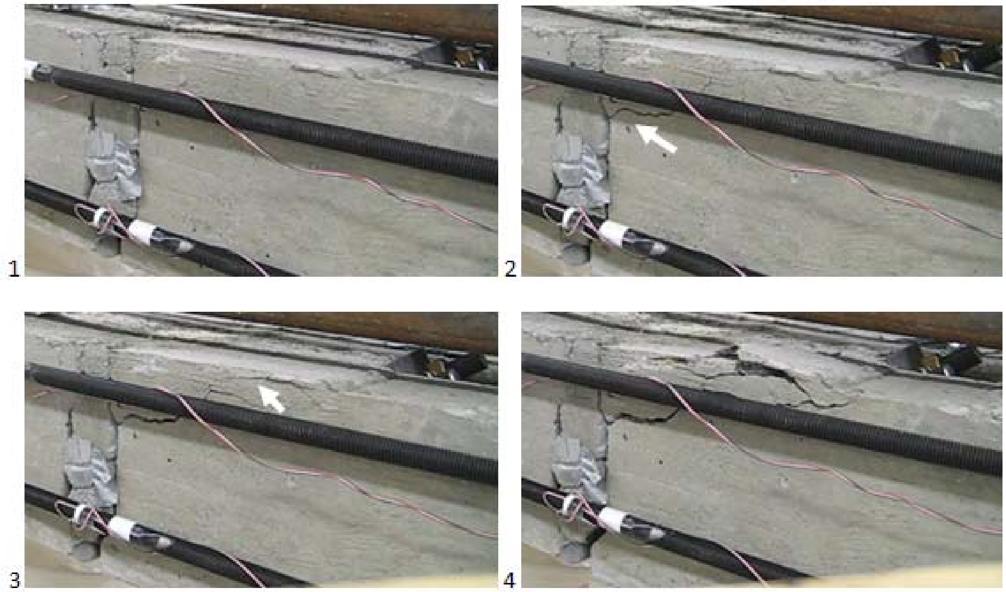

Figure 41. Cracking sequence of a 24-inch curved bolt flexural laboratory specimen.

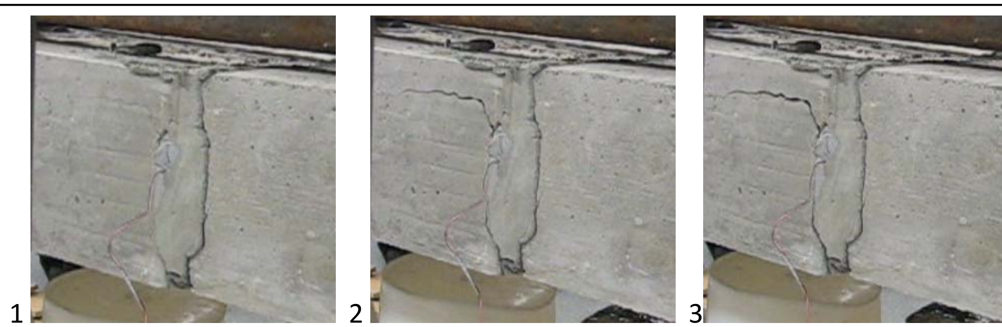

Figure 42. Cracking sequence of a 36-inch curved bolt flexural laboratory specimen.

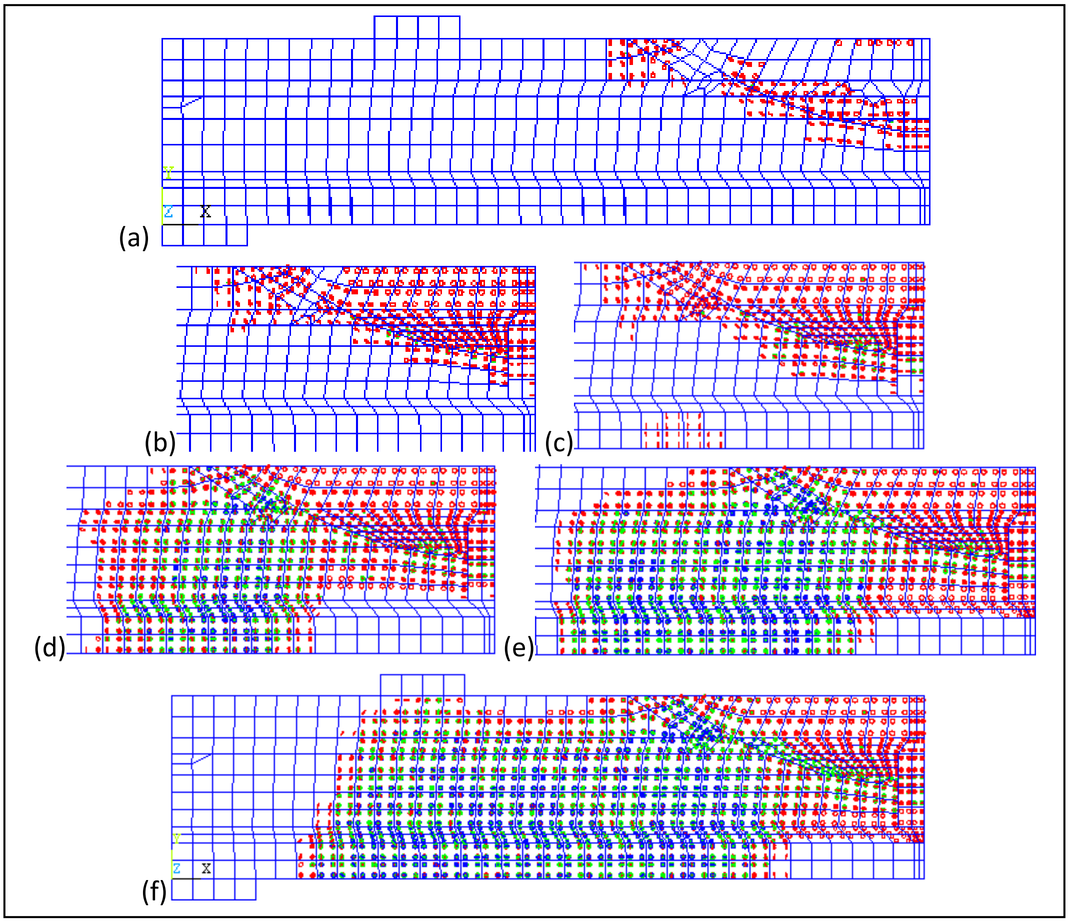

Figure 43. Cracking sequence of the 24-inch curved bolt flexural finite element model.

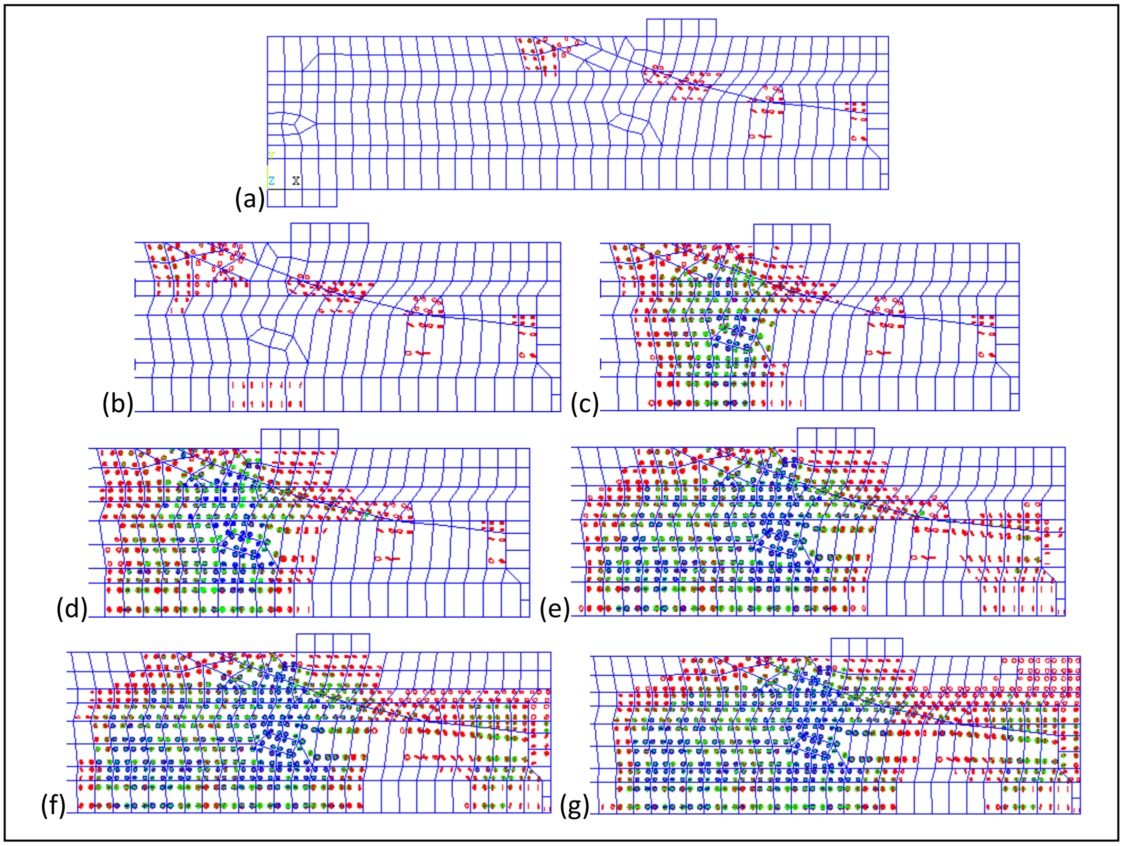

Figure 44. Cracking sequence of the 36-inch curved bolt flexural finite element model.

THIS PAGE INTENTIONALLY LEFT BLANK

6.0 CONCLUSIONS

Full scale monotonic and cyclic push-off shear testing of four precast bridge deck panel transverse connections and full scale positive moment flexural testing of five precast bridge deck panel transverse connections were performed to determine the cracking and ultimate strengths of these connection details. For each connection, cracking, deflections, and moments were recorded. Additionally, non-linear finite-element models were created for each connection detail. The finite-element results were compared with the experimental values. The following conclusions were obtained based on the results.

The welded stud connection was weak in moment with only 0.39 times the capacity of the post tensioned connection. In shear, the welded portion of this connection was strong with 0.87 times the strength of the post tensioned connection; however, the unreinforced regions of the connection significantly reduce its strength making more realistic capacities around 0.4 to 0.5 times the post tensioned connection's capacity. Cracking loads in shear and flexure were both low for this connection.

The welded rebar connection used on a bridge on I-84 in Utah was found to be much stronger than the welded stud connection in both shear and flexure. In shear, the test specimens always failed away from the connection providing inconclusive results but suggesting that the connection has great shear strength. In flexure, the welded rebar connection had 2.7 times the ultimate capacity of the welded stud connection. It failed at 1.1 times the moment the post tensioned connection held. The connection did not have the pulling out problems that the welded stud connection had. In addition, the rebar connection started cracking at more than double the flexural load causing cracking of the welded stud connection and at 0.88 times the load required to crack the post tensioned connection. This shows that the welded rebar connection may be a good option to gain added strength and durability without post tensioning.

The post tensioned connection was stronger than the welded stud connection in both shear and flexure. It held about 1.2 times the shear load required to fail a continuously welded stud connection and 1.3 times the shear load required to fail a welded stud specimen spaced at 18 inches on center. In flexure the connection held 2.6 times the moment as the welded stud connection. The post tensioning was found to increase this connection's shear strength by a factor of 4. Not only did the post tensioned connection have higher ultimate capacities than other connections, but it also cracked under higher loads. The earliest recorded cracking of this connection in shear was 3.3 times that required to crack the welded portion of the welded stud connection and 6.6 times that required to crack the unreinforced portion of the welded connections. In flexure, this connection cracked at 2.4 times the load required to crack the welded stud connection.

Both curved bolt connections failed at higher flexural loads than the welded stud connection. Of the two curved bolt lengths tested, the longer bolt performed better. It failed at 1.7 times the load required to fail the shorter curved bolt and at 1.2 times the load required to fail the post tensioned connection. It is believed that the long curved bolt was stronger than the post tensioned connection because the panel concrete was stronger in the long curved bolt specimens. In reality the long curved bolt would have about the same or slightly less strength as the post tensioned connection. The 24-inch curved bolt started cracking at around 3000 lb-ft, or essentially the same load that cracked the welded stud connection and only about 0.4 times the load required to crack the post tensioned connection. The 36-inch connection cracked at much higher loads, about 0.76 times those required to crack the post tensioned connection. This shows that using curved bolts may be an effective way to post tension bridge decks in the future, but emphasizes the need to choose the proper bolt geometry. Another advantage of these connections is that their short length should reduce problems with creep and prestress losses as compared to traditionally post tensioned connections.

Cyclic shear testing was largely inconclusive. It implied that most connections can withstand over 30 cycles of high amplitude cyclic loading without failure. Testing did not evaluate the long term fatigue behavior of any connections.

Finite element models closely followed the monotonic shear and flexural laboratory results. Similar shear-deflection and moment-deflection curves were produced using finite element and laboratory testing. Similar cracking (loads, sequences and locations) was also observed using FE analysis in most cases.

The finite-element analysis shows internal cracking with both the welded stud and welded rebar connections at loads 5 times less than in the post tensioned FE model. Post tensioning reduces the internal cracking of the specimens.

From the finite-element results the post tensioned connection demonstrated the best behavior, and the highest cracking moment of 18,940 N-m (13,980 lb-ft), approximately 1.1 times the highest tested cracking moment.

THIS PAGE INTENTIONALLY LEFT BLANK

7.0 RECOMMENDATIONS/IMPLEMENTATIONS

The welded stud and welded rebar connections should both be studied in long term fatigue with realistic traffic loads to determine if their welds have fatigue problems.

To better understand the welded rebar connection, a field study should be done on bridges using this connection, particularly the bridge on I-84 in Weber Canyon. This connection is also recommended for use in bridges as an alternative to the current welded stud connection.

The curved bolt connection should be studied further before being implemented in bridges. Research needs to be done to determine the time dependent behavior of the connection including post tensioning losses. Also, research should be done to determine the best lengths for the connection and spacing for the bolts. The connection should be tested in negative moment to determine the feasibility of using this connection for multi-span bridges. Research could also be done to determine if connecting the bolts from the top or the bottom of the panels makes any difference. Eventually, a prototype bridge using the curved bolt connection should be constructed and tested to determine how the connection behaves on a complete bridge as well as the long term fatigue strength of the connection.

THIS PAGE INTENTIONALLY LEFT BLANK

APPENDICES

APPENDIX A – TESTING DATA

Table 6. Deck Panel Concrete 28 Day Strengths

Date Cast	28 day f'c (psi)	28 day tensile strength (psi)
8/7/2008	5389	486
8/7/2008	5521	486
8/7/2008	5370	---
8/7/2008 average	**5427**	**486**
8/27/2008	6999	472
8/27/2008	7136	486
8/27/2008	7204	446
8/27/2008 average	**7113**	**468**
9/18/2008	5811	509
9/18/2008	6264	---
9/18/2008	6123	---
9/18/2008 average	**6066**	**509**

Table 7. Grout Compressive Strengths

Date Cast	Batch	Cylinder	1 day f'c (psi)	2 day f'c (psi)	3 day f'c (psi)
10/23/2008	1	1	3140		
		2			5028
	2	1	4500		
		2	4527		
		3			6659
		4			6111
10/27/2008*	1	1	4321		
		2	4206		
		3			6175
10/29/2008	1	1	4281		
		2	4336		
		3		5681	
11/5/2008	1	1	3763		
		2		5534	
		3		5823	
11/12/2009	1	1	4169		
		2	3854		
		3		5607	
12/1/2009	1	1	4251		
		2	4011		
		3		>5000	
1/7/2009	1	1	3587		
	1	2		5616	
	1	3		5433	
	2	1	3305		
	2	2		5262	
	2	3		5629	

* All welded specimens grouted on 10/23/08 were patched with this grout

Table 8. Test Specimen Information

Test	Connection	Specimen #	Date Cast	Date Grouted	Date Tested
Monotonic Shear	WS	1	8/27/2008	10/23/2008*	12/5/2008
		2	8/27/2008	10/23/2008*	12/10/2008
		3	9/18/2008	10/23/2008*	12/11/2008
	UR	1	9/18/2008	10/27/2008	12/5/2008
		2	8/27/2008	10/27/2008	12/10/2008
		3	8/7/2008	10/27/2008	12/1/2008
		4	9/18/08	11/5/2008	12/15/2008
	NPT	1	8/27/2008	11/5/2008	12/11/2008
		2	9/18/2008	10/29/2008	12/10/2008
	PT	1	8/7/2008	11/5/2008	12/11/2008
		2	8/27/2008	11/5/2008	12/15/2008
		3	9/18/2008	10/23/2008	12/3/2008
Cyclic Shear	WS	1	9/18/2008	10/27/2008	12/16/2008
		2	8/7/2008	10/23/2008	12/18/2008
	UR	1	8/27/2008	10/27/2008	12/16/2008
		2	9/18/2008	1/7/2008 2nd	1/9/2009
	NPT	1	8/7/2008	11/5/2008	12/17/2008
	PT	1	9/18/2008	11/5/2008	12/23/2008
		2	8/7/2008	11/5/2008	12/18/2008
		3	8/7/2008	11/5/2008	1/5/2009
		4	8/27/2008	10/27/2008	1/6/2009
Flexure	WS	1	8/7/2008	11/2/2008	1/26/2009
		2	9/18/2008	10/27/2008	1/20/2009
		3	8/27/2008	12/1/2008	2/4/2009
	WR	1	8/7/2008	11/12/2008	2/20/2009
		2	8/27/2008	12/1/2008	2/9/2009

	3	9/18/2008	11/12/2008	2/20/2009
PT	1	8/27/2008	1/7/2009	2/25/2009
	2	8/7/2008	1/7/2009	2/24/2009
	3	8/7/2008	10/23/2008	1/30/2009
	4	8/7/2008	1/7/2009	2/27/2009
24CB	A	9/18/2008	12/1/2008	1/22/2009
	1	9/18/2008	1/7/2009 2nd	2/9/2009
	2	8/27/2008	1/7/2009	2/11/2009
36CB	1	9/18/2008	12/1/2008	2/3/2009
	2	9/18/2008	12/1/2008	2/18/2009
	3	9/18/2008	1/7/2009 2nd	2/13/2009

*patched with 10/27/2008 grout

Table 9. Shear Specimen Monotonic Ultimate Capacities

Connection	Specimen #	Concrete f'c (psi)	Ultimate Capacity (lbs)
Welded Stud	1	7113	19042
	2	7113	20327
	3	6066	24657
	Average		**21342**
Welded Rebar	---	---	Failed away from connection
Unreinforced Portion for Welded Connections	1	6066	5157
	2	7113	6324
	3	5426	10589
	4	6066	8434
	Average		**7626**
Non-Post Tensioned	1	7113	5282
	2	6066	7451
	Average		**6367**
Post Tensioned	1	5426	16602
	2	7113	26532
	3	6066	30883
	Average		**24672**

Table 10. Shear Specimen Cracking

Connection	Specimen #	Cracking Load (lbs) (approximate)	Notes
Welded Stud	1	---------	---------
	2	5000	Cracking along stud and grout separation on left side (bottom)
		11200	More cracking
		17000	Major cracking all the way through specimen
		21000	Cracks all the way through specimen on right side (top)
	3	14500	Cracking along stud
		18000	Large cracks
Unreinforced Portion for Welded Connections	1	--------	--------
	2	2500	Crack along grout interface on bottom followed by a diagonal crack in concrete from connection corner
		5000	Diagonal crack spreads through grout and concrete immediately before failure
	3	---------	---------
	4	3400	Cracks form along grout interface
Non-Post Tensioned	1	4000	Crack along grout interface and diagonally into concrete from bottom pocket corner
	2	7000	Sudden diagonal crack through concrete, grout, and interface between concrete and grout followed by immediate failure

Post Tensioned	1	16500	Continuous diagonal crack through grout and concrete on one side, going vertical along grout interface for a portion of other side, then diagonal again
	2	26000	Crack along grout interface followed very shortly by crack through panel and ultimate failure
	3	---------	---------

Table 11. Flexural Specimen Capacities

Connection	Specimen #	Panel f'c (psi)	Ultimate Flexural Capacity (lb-ft)
Welded Stud	1	5427	4509
	2	6066	6835
	3	7113	8657
	Average		**6667**
Welded Rebar	1	5427	14528
	2	7113	22339
	3	6066	17274
	Average		**18047**
Post Tensioned	1	7113	16028
	2	5427	14973
	3	5427	21182
	4	5427	16861
	Average		**17261**
24-inch Curved Bolt	A*	6066	6547
	1	6066	15511
	2	7113	8647
	Average		**12079**
36-inch Curved Bolt	1	6066	17450
	2	6066	23053
	3	6066	21366
	Average		**20623**

*The strain gage stopped working just before reaching full strain. Results are approximate. Data not used for average.

Table 12. Flexural Specimen Cracking

Connection	Specimen #	Cracking Load (lb-ft) (approximate)	Notes
Welded Stud	1	1000	Grout separating
		4100	Bad cracking
	2	2600	Cracking heard
		3350	Cracks seen at location of stud and underside
	3	3350	Crack on pocket corner in panel going up and parallel to connection at end of stud on underside.
		7100	Large crack parallel to connection at end of stud on underside
Welded Rebar	1	13700	Small cracks coming from connection corners
	2	4000	Heard something
		16200	Crack from pocket visible
	3	7200	Hairline
		15700	Heard large cracking
Post Tensioned	1	8200	Cracking
		11200	Connection separating
		14200	Cracks in grout noticed
	2	12700	Cracks near top of grout and spreading from connection
		14700	Crack on corner of grout pocket in panel
	3	10200	Cracks across grout and tiny cracks across connection edge

		13200	Large connection separation
	4	--------	--------
24-inch Curved Bolt	A*	5600	Crack along curved bolt
	1	3100	Cracks start
	2	3350	Cracks across grout
		6100	Cracks along curved bolt
36-inch Curved Bolt	1	8200	Cracks seen and heard along bolt
	2	6200	Crack in grout and top of connection
		7450	Major separation of connection
	3	4700	Cracking heard
		10200	Cracks seen
		17700	Large crack along bolt

*The strain gage stopped working just before reaching full strain. Results are approximate.

APPENDIX B: PHOTOS OF SPECIMENS AFTER TESTING

Figure 45. Ultimate cracking of welded stud shear specimens.

Figure 46. Ultimate cracking of unreinforced shear specimens for welded connections.

Without 300 psi Applied Compression

With no applied compression (no post-tensioning)

Figure 47. Ultimate cracking of post tensioned type shear specimens.

Figure 48. Ultimate cracking of welded stud flexural specimens.

Figure 49. Ultimate cracking of welded rebar flexural specimens.

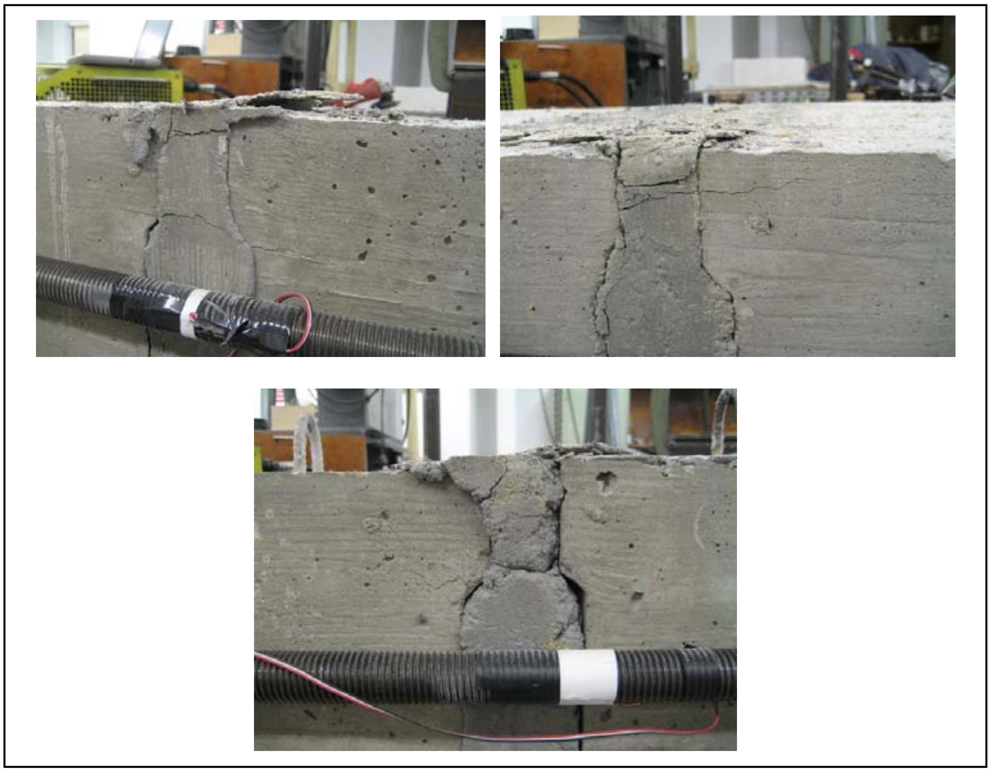

Figure 50. Ultimate cracking of post tensioned flexural specimens.

Figure 51. Ultimate cracking of 24-inch curved bolt flexural specimens.

Figure 52. Ultimate cracking of 36-inch curved bolt flexural specimens.

REFERENCES

Badie, S. S., Baishya, M.C., Tadros, M. K. (1998a). “NUDECK – An efficient and economical precast bridge deck System.”, *PCI J.*, 43(5), September-October, 56-74.

Badie, S. S., Baishya, M. C., Tadros, M. M. (1998b). “NUDECK – A new prestressed stay-in-place concrete panel for bridge decks.” *Proc., 1998 Transportation Conference*, University of Nebraska-Lincoln, Lincoln.

Badie, S. S., and Tadros, M. K. (2008). *Full-depth precast concrete bridge deck systems*. National Cooperative Highway Research Program Report 584, Transportation Research Board of the National Academies, Washington, D.C.

Bakhoum, M. M. (1991). “Shear behavior and design of joints in precast concrete segmental bridges.” PhD thesis, Massachusetts Institute of Technology, Cambridge.

Biswas, M. (1986). “Precast bridge deck design systems.” *PCI J.*, 31(2), March-April, 40-94.

Brush, C. N. (2004). “Connection of modular steel beam precast slab units with cast-in-place closure pour slab.” M.S. thesis, Texas A&M University, College Station.

Fallaha, S., Sun, C., Lafferty, M. D., Tadros, M. K. (2004). “High performance precast concrete NUDECK panel system for Nebraska’s Skyline Bridge.” *PCI J.*, 49(5) September-October, 40-50.

Gordon, S. R., and May, I. M. (2006). “Development of in situ joints for pre-cast bridge deck units.” *Bridge Engineering Institute* (BEI), Issue 159, March, 17-30.

Gulyas, R. J., Wirthlin, G. J., Champa, J. T. (1995). "Evaluation of keyway grout test methods for precast concrete bridges." *PCI J.*, 40(1), January-February, 44-57.

Issa, M. A., Idriss, A.-T., Kaspar, I. I., Khayyat, S. Y. (1995a). "Full depth precast and precast, prestressed concrete bridge deck panels." *PCI J.*, 40(1), January-February, 59-80.

Issa M. A., Yousif, A. A., Issa, M. A., Khayyat, S. Y. (1995b). "Field performance of full depth precast concrete panels in bridge deck reconstruction." *PCI J.*, 40(3), May-June, 82-108.

Issa, M. A., Ribiero do Valle, C. L., Abdalla, H. A., Islam, S., Issa, M. A. (2003). "Performance of transverse joint grout materials in full-depth precast concrete bridge deck systems.", *PCI J.* 48(4), July-August, 92-103.

Kim, Y.-C., Shin, S., Park, J.-J. (2003). "Shear and fatigue strength of grout-type transverse joints." *Canadian J. of Civil Eng.*, 30, 607-614.

Markowski, S. M., (2005). "Experimental and analytical study of full-depth precast/prestressed concrete deck panels for highway bridges." M.S. thesis, University of Wisconsin-Madison, Madison, Wis.

Oliva, M. G., Bank, L. C., Russell, J. S., Markowski, S., Ehmke, G., Chi, S. J. (2007). *Full depth drecast concrete highway bridge decks*. Structures and Materials Test Laboratory, College of Engineering, University of Wisconsin, Madison.

Ryu, H.-K., Kim, Y.-J., Chang, S.-P. (2007). "Experimental study on static and fatigue strength of loop joints." *Engineering Structures*, 29, 145-162.

Shim, C.-S., Chung, C.-H., Hyun, B.-H., Kim, I.-K., Kim, Y.-J. (2005). "Experimental research on the connection for prefabricated bridges." *Proc. FHWA Conference 2005*, 12, 184-189.

Sullivan, S. (2007). "Construction and behavior of precast bridge deck panel systems." PhD dissertation, Virginia Polytechnic Institute and State University, Blacksburg, Va.

UDOT. (2007). "I-84: US-89 to SR-167, Weber Canyon." Bridge Deck Replacement Plans, UDOT Structures Division, Salt Lake City, Utah.

UDOT. (2008a). "ABC standards." <http://www.dot.state.ut.us/main/uconowner.gf?n=1966945409050115798> Full Depth Precast Concrete Deck Panel Standard Drawings, UDOT Structures Division, Salt Lake City, Utah.

UDOT. (2008b). "Full depth precast concrete deck panel detailing manual." < http://www.dot.state.ut.us/main/f?p=100:pg:0::::T,V:2090,> (April 4, 2009) UDOT Structures Division, Salt Lake City, Utah.

UDOT. (2008c). "Full depth concrete deck panels special provision." < http://www.dot.state.ut.us/main/f?p=100:pg:0::::T,V:2090,> (April 4, 2009) UDOT Structures Division, Salt Lake City, Utah.

Yamane, T., Tadros, M. K., Badie, S.S., Baishya, M.C. (1998). "Full depth precast, prestressed concrete bridge deck system." *PCI J.*, 43(3), May-June, 51-65.

Yousif, A. A. (1998). "Experimental behavior of full depth precast concrete deck panels for bridge reconstruction." PhD thesis, University of Illinois at Chicago.

THIS PAGE INTENTIONALLY LEFT BLANK

ACRONYMS

ABC	accelerated bridge construction
LVDT	linear variable displacement transducer
UDOT	Utah Department of Transportation
USU	Utah State University